Active deformation in the Mediterranean from Gibraltar to Anatolia inferred from numerical modeling and geodetic and seismological data

I. Jiménez-Munt, R. Sabadini, and A. Gardi[1]
Sezione Geofisica, Dipartimento di Scienze della Terra, Università di Milano, Italy

G. Bianco
Agenzia Spaziale Italiana, Centro di Geodesia Spaziale "G. Colombo,", Matera, Italy

Received 9 October 2001; revised 29 April 2002; accepted 9 May 2002; published 3 January 2003.

[1] From Gibraltar to Anatolia, the active tectonics in the Mediterranean is studied by means of an integrated approach based on geophysical, geodetic, and seismological methodologies. The aim of this study is to gain a deep insight into the kinematics and dynamics of the crustal and lithospheric processes affecting the Mediterranean. Major tectonic processes, such as continental collision and subduction, characterize this region, which marks a broad transition zone between the African/Arabian and Eurasian plates. A thin-shell finite element approach allows us to simulate the deformation pattern in the Mediterranean, from 10°W to 40°E and from 30° to 50°N. The global plate motion model NUVEL-1A is used to account for the convergence, while the relative velocities of the overriding and subduction plates are obtained from another family of models. These models simulate the effects of the negatively buoyant density contrasts of the subducted lithosphere on the horizontal velocity at the surface. A systematic comparison between model results and the seismic strain rates obtained from the National Earthquake Information Center catalog, the geodetic velocity field and strain resulting from GPS, satellite laser ranging, and very long baseline interferometry analyses and the World Stress Map, indicate that Africa/Arabia versus Eurasia convergence and subduction in the Aegean Sea and Calabrian Arc are the major tectonic mechanisms controlling the deformation style in the Mediterranean. It is shown that in order to carry into coincidence the modeled and the seismic strain rate patterns and the geodetically retrieved strain rate tensors, a deep subduction in the Aegean Arc must be included in the modeling. *INDEX TERMS:* 8120 Tectonophysics: Dynamics of lithosphere and mantle—general; 8107 Tectonophysics: Continental neotectonics; 8123 Tectonophysics: Dynamics, seismotectonics; *KEYWORDS:* neotectonics, finite elements, strain rate, seismicity

Citation: Jiménez-Munt, I., R. Sabadini, A. Gardi, and G. Bianco, Active deformation in the Mediterranean from Gibraltar to Anatolia inferred from numerical modeling and geodetic and seismological data, *J. Geophys. Res.*, *108*(B1), 2006, doi:10.1029/2001JB001544, 2003.

1. Introduction

[2] The tectonic setting of the Mediterranean is dominated by subduction in the Hellenic and Calabrian Arc and by collision between the African and Arabian plates with Eurasia [e.g., *McKenzie*, 1970; *Jackson and McKenzie*, 1988]. This region exhibits various processes, from continental collision to escape tectonics with major continental strike-slip faults, subduction of continental and oceanic lithosphere and associated back arc spreading. Figure 1 is a sketch of the major tectonic structures under study, including the topographic elevation, with the solid line indicating the Africa-Eurasia plate boundary and major faults, like the North Anatolian Fault (NAF), East Anatolian Fault (EAF), and South Anatolian Fault (SAF). In spite of the Africa/Arabia versus Eurasia convergence, several regions exhibit extension, such as the Alboran Sea, the Algero-Provençal Basin, and the Tyrrhenian and the Aegean Seas. This combination of convergence and extension has been an enigmatic feature of the region. New geological and geophysical data are gradually being integrated into tectonic reconstructions. Studies of deep structure [e.g., *Du et al.*, 1998; *Bijwaard and Spakman*, 2000] and heat flow data [*Pollack et al.*, 1993] reveal distinct differences between the lithosphere in the western central Mediterranean (from the Alboran to Tyrrhenian Seas) and those in the eastern Med-

[1]Now at Institut de Protection et Sûreté Nucléaire, Fontenay-aux-Roses, France.

0148-0227/03/2001JB001544$09.00

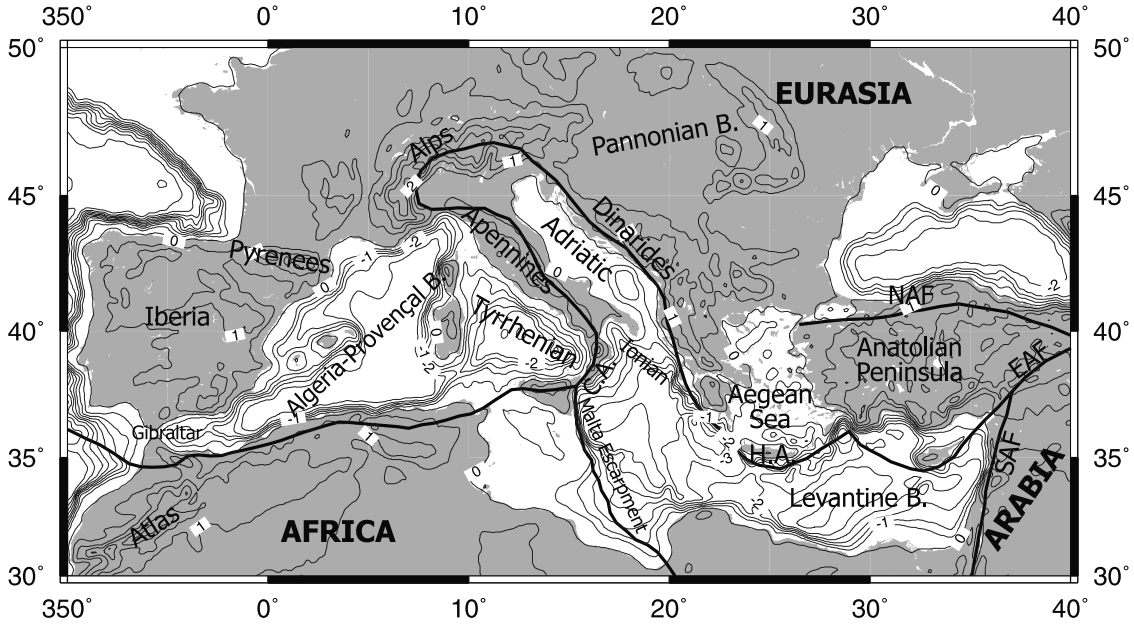

Figure 1. Elevation (ETOPO5), in kilometers with isolines every 0.5 km, and tectonic sketch map of the study region. H.A., Hellenic Arc; C.A., Calabrian Arc; B, basin; NAF, North Anatolian Fault; SAF, South Anatolian Fault; EAF, East Anatolian Fault.

iterranean (Ionian, Adriatic, and Levantine Basins, Figure 1). The eastern Mediterranean basins are part of the African plate, formed in the Mesozoic. The western basins constitute a deformed plate boundary region of the Eurasian plate, created by back-arc extension in the late Oligocene to recent times [*Doglioni et al.*, 1997; *Wortel and Spakman*, 2000]. The idea of a land-locked basin setting provides the framework for a dynamical analysis of some Mediterranean zones [*Le Pichon and Angelier*, 1979; *Gueguen et al.*, 1998; *Wortel and Spakman*, 2000]. It leads to rollback and to consumption of the oceanic lithosphere between Africa and Eurasia and to extension in the overriding plate above the subduction zones. Earthquakes in the Mediterranean are not confined to a single fault, implying that the deformation in this region cannot be described simply by the relative motion between rigid blocks. Within the broad deforming belts in the continents some large, flat, aseismic regions such as central Turkey or the Adriatic Sea, appear to be rigid and can usefully be thought of as microplates [e.g., *Jackson and McKenzie*, 1984; *Ward*, 1994]. However, in most continental areas the scale on which the active deformation and its consequent topographic features, such as mountain belts, plateaus, and basins, are distributed, makes it more practical to describe the overall characteristics of that deformation by a velocity field, rather than by the relative motions of rigid blocks. An important problem is then to obtain this velocity field and to understand its relation to the motions of the rigid plates that bound the deforming region and its relation to the forces involved in the deformation.

[3] A major advance in the last decade has been made in estimating such velocity fields either from GPS measurements [e.g., *Clarke et al.*, 1998; *McClusky et al.*, 2000], from fault slip rates [e.g., *England and Molnar*, 1997], or from spatial variations in strain rates [e.g., *Holt et al.*, 1991; *Jiménez-Munt et al.*, 2001a]. Thus, for example, attempts have been made to understand how the velocity field in the Mediterranean region is related to the convergence between Africa/Arabia and Eurasia [e.g., *Jackson and McKenzie*, 1984; *Taymaz et al.*, 1991; *Jackson*, 1992; *Ward*, 1994; *McClusky et al.*, 2000], while little is known about the relative importance of the driving forces either due to push forces acting at the edge of the plate or to pull forces induced by the foundering plate. The present work focuses on the numerical modeling of the major tectonic processes active in the Mediterranean and on the comparison between model predictions and geodetic, seismic and stress data. In the present analysis, the modeling includes convergence between the Africa/Arabia and Eurasia plates and the additional forces acting at plate boundaries due to subduction.

[4] Our study builds on a series of previous modeling efforts that focused on selected parts of the Mediterranean. By means of a thin-sheet viscous model of the central Mediterranean, *Bassi and Sabadini* [1994] and *Bassi et al.* [1997] first showed that subduction of the Ionian lithosphere underneath the Calabrian Arc is necessary to account for the extensional style in the Tyrrhenian Sea, within the context of convergence between Africa and Eurasia. For the same region considered by *Bassi et al.* [1997], *Negredo et al.* [1999] have shown the effects of three-dimensional subduction structures in controlling the retreat velocity along the hinge of subduction.

[5] Other studies have focused on the kinematics and stress pattern in the Aegean region within two-dimensional (2-D) elastic thin-shell modeling [*Meijer and Wortel*, 1996; *Lundgren et al.*, 1998], while *Cianetti et al.* [1997] made use of a viscous thin-sheet model. *Giunchi et al.* [1996b] have shown, using 2-D models of subduction in a vertical plane perpendicular to the subduction arc, the effects of relative plate velocities in the Aegean Sea on the stress pattern that has a major influence on the earthquakes distribution with depth and on the interpretation of sea level data in the island of Crete.

[6] In the present analysis we overcome difficulties encountered in these previous studies associated with the limited spatial extent of the modeled domain. Previous models did not allow for self-consistent boundary conditions at the edges of the studied area. In contrast, we model simultaneously for the entire Mediterranean, the effects of Africa/Arabia-Eurasia convergence from Gibraltar to Anatolia, including the effects of subduction in the Calabrian Arc and in the Aegean Sea and the effects of slip along the whole plate boundary separating Africa/Arabia and Eurasia. In comparison to previous studies, we now also have at our disposal a large amount of geodetic data. These data permit a comparison between the modeled strain rate and the geodetic one, and this provides a robust test for our hypotheses regarding tectonic driving mechanisms.

2. Methodology

[7] We use the thin-shell neotectonic modeling program SHELLS [*Kong and Bird*, 1995]. The thin-plate method of modeling the deforming lithosphere uses isostasy and vertical integration of lithospheric strength to reduce three-dimensional problems to two dimensions, where the horizontal velocity components do not depend on the depth. The horizontal components of the momentum equation are vertically integrated through the plate and are solved using a 2-D finite element grid. Therefore only the horizontal components of velocity are predicted. The thin shell is based on spherical shell elements that can handle regional and global problems. The vertical component of the momentum equation is obtained from the assumption of isostatic equilibrium. Therefore vertical normal stress is lithostatic at all points, assuming no vertical shear traction on vertical planes [*Bird*, 1989]. The basic equation that SHELLS solves is the Newtonian conservation of momentum. When the only body forces arise from the gravitational acceleration, this equation may be written as

$$\rho \frac{d\mathbf{u}}{dt} = \nabla\sigma + \rho\mathbf{g}, \tag{1}$$

where $\mathbf{u}$ is the velocity vector, t is time, ρ is the density, σ is the stress tensor, and $\mathbf{g}$ is the gravitational acceleration. In dealing with slow tectonic processes we can neglect the acceleration $d\mathbf{u}/dt$ in equation (1). With the assumption that the vertical normal stress is lithostatic, this stress can be written as

$$\sigma_{zz} = -g \int_{z_0}^{z} \rho(z) dz, \tag{2}$$

where z_0 is at the land or sea surface and z is the depth. Therefore the finite element method is required only to solve for the horizontal components of the momentum equation. The usual thin-plate approximation integrates the equilibrium equation (1) in all the layers and assumes that only the net forces transmitted laterally are significant. This leads to

$$\int_{z_0}^{z} \frac{\partial \sigma_{ij}}{\partial x_j} dz = 0 \quad i,j = 1,2. \tag{3}$$

[8] The rheology has the same mathematical form at all points [*Bird*, 1989]. The code neglects all elastic strain accumulation and release and solves for velocities, fault slip rates, and anelastic strain rates and stresses. Deformation occurs by frictional sliding or nonlinear dislocation creep. Given a strain rate, the deviatoric stress is evaluated separately for each of three flow laws: frictional faulting, dislocation creep (power law), and Newtonian creep (linear). At each point, the flow law that provides the lowest maximum shear stress is selected. The dislocation creep (power law) rheology is given by

$$\sigma_{\text{creep}} = \left\{ 2A \left[2(-\dot{\epsilon}_1\dot{\epsilon}_2 - \dot{\epsilon}_1\dot{\epsilon}_3 - \dot{\epsilon}_2\dot{\epsilon}_3)^{1/2} \right]^{(1-n)/n} \exp\left(\frac{B + Cz}{T} \right) \right\} \dot{\epsilon}, \tag{4}$$

where $\dot{\epsilon}$ is the strain rate tensor and T is the absolute temperature. The values adopted for the rheological parameters A, B, and C are different for the crust and mantle lithosphere. The rheological parameters impose the lithospheric rigidity and the coupling between the crust and the lithospheric mantle. As we are studying a large area, with different types of lithosphere, we have chosen the parameters that represent an average lithosphere. The crustal rheology is based on neotectonic models [*Bird and Kong*, 1994], with $A = 2.3 \times 10^9$ Pa $s^{1/3}$, $B = 4000$ K, $C = 0$ K m^{-1}, and $n = 3$. The mantle rheology is based on the studies of olivine deformation summarized by *Kirby* [1983] for a dry rheology, with $A = 9.5 \times 10^4$ Pa $s^{1/3}$, $B = 18314$ K, $C = 0.017$ K m^{-1}, and $n = 3$. Frictional faulting stress is evaluated under the assumption of hydrostatic pore pressure

$$\sigma_f = \mu_f(-\sigma_n - P_w), \tag{5}$$

where σ_n is the normal stress, μ_f is the coefficient of friction, and P_w is the pore pressure. Faults are distinguished from continuum elements only by their shape and lower coefficient friction. The coefficient of friction is the same in the continuum parts of the crust and mantle-lithosphere layers ($\mu_f = 0.85$), but a lower value is usually assigned to fault elements. In order to simulate plate boundaries the method makes use of double nodes with a lower frictional coefficient with respect to the continuum medium.

[9] The method incorporates some 3-D characteristics since volume integrals of density and strength are performed numerically in a lithosphere model with laterally varying crust and mantle-lithosphere layer thicknesses, heat flow, and elevation. To determine the crustal and lithospheric mantle structure, we have assumed local isostasy and steady state thermal regime with the base of the lithosphere defined by the 1350°C isotherm. Under these conditions, there is a relationship between absolute elevation, surface heat flow, crustal thickness, and lithospheric mantle thickness, so that the knowledge of any two of these variables usually allows us to specify all the four quantities [*Jiménez-Munt et al.*, 2001a].

3. Lithosphere Structure

[10] The plane stress approach treats the lithosphere as a thin layer with a vertically averaged rheology. This average rheology is calculated at each node of the finite element grid on the basis of the crustal and the lithospheric mantle thicknesses. We make use of the elevation and surface heat

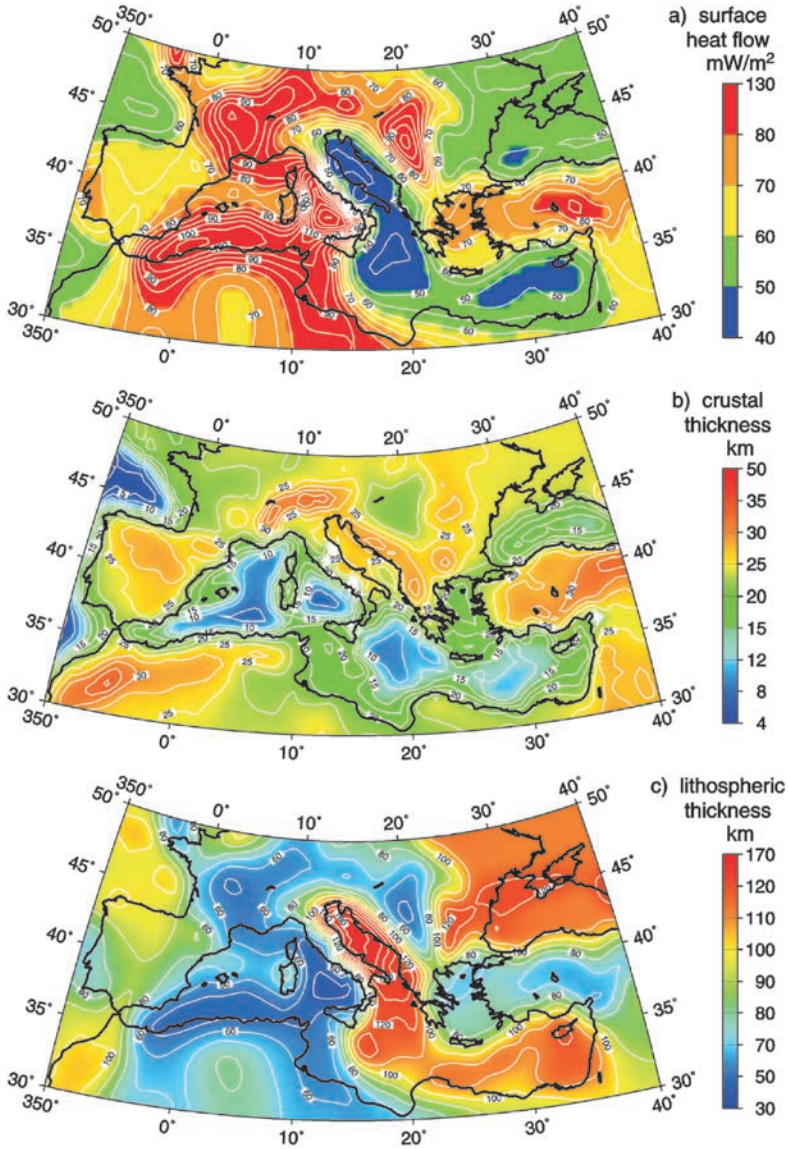

Figure 2. (a) Surface heat flow data (mW m^{-2}) from *Pollack et al.* [1993] completed with data from *Fernandez et al.* [1998], contours every 5 mW m^{-2}. (b) Calculated crustal thickness, contours every 2.5 km. (c) Calculated lithospheric thickness, contours every 10 km.

flow data to determine the lithospheric structure and its thermal structure under the assumption of local isostasy and a steady state thermal regime. The elevation is taken from the ETOPO5 global data set, with data every 5′ (Figure 1), with isolines providing the topography in kilometers. The surface heat flow is taken from the global data set of *Pollack et al.*, [1993] augmented by data obtained by *Fernandez et al.* [1998] for the Iberian Peninsula and Alboran Sea (Figure 2a). Table 1 summarizes the mean crustal and lithospheric parameters used to calculate the regional crustal and lithospheric thickness variations shown in Figures 2b and 2c. The calculations have been performed after filtering all the observables, with the aim of removing local features. These maps (Figures 2b and 2c) do not reflect the fine structure of the crust and mantle lithosphere, although the resolution we have adopted is responsible for the appearance of important lateral variations in the total lithospheric strength. Assuming local isostasy can result in the misestimation of the actual lithosphere structure. However, the induced departures in the calculated lithospheric strength and the gravitational potential energy are negligible, and hence local isostasy is a valid approach for the purposes of this study. The thickness of the crust (Figure 2b) varies approximately between 5 and 50 km. Minimum crustal thicknesses of about 5–15 km are found in the oceanic domains, namely, in the Algero-Provençal Basin, Tyrrhenian Sea, Ionian Sea, and Levantine Basin. The crust is thicker under the orogenic belts, Atlas, Alps, Dinarides, and east Anatolian Peninsula. A significant crustal thinning is observed in the Pannonian Basin. The lithospheric thickness (Figure 2c) reaches minimum values in the Algero-Provençal Basin and Tyrrhenian Sea. In contrast, in the eastern part of the Mediterranean (Ionian and Adriatic Sea and Levantine Basin) a thicker lithosphere is necessary in

Table 1. Model Parameters for the Crust and Lithospheric Mantle

Parameter	Crust	Lithospheric Mantle
Mean density at $P = 0$, $T = 0$, kg m^{-3}	2800	3350
Volumetric thermal expansion coefficient, K^{-1}	0	3.5×10^{-5}
Thermal conductivity, W (mK)$^{-1}$	3.0	3.4
Radioactive heat production, W m^{-3}	0.7×10^{-6}	0

order to explain the low measured surface heat flow. This difference between the eastern and western Mediterranean lithosphere is also observed by *P* wave studies [*Bijwaard and Spakman*, 2000] and surface wave tomography [*Du et al.*, 1998]. The crustal and lithospheric thicknesses agree with the seismologically retrieved ones of EurID [*Du et al.*, 1998] and *Ansorge et al.* [1992]. Deviations between our lithosphere thickness and the seismological one could arise from several causes: a different treatment of the lithosphere, in our case defined by the isotherm of 1350°C, possible errors in surface heat flow data, or the assumption of local isostasy. However, these variations in the structure of the lithosphere have little effect on the lithospheric strength and gravitational energy, which makes our lithospheric structure adequate for neotectonic studies.

4. Seismic, Geodetic, and Stress Data

[11] The testable predictions of each model experiment include seismic, geodetic, and stress data, as given hereafter.

4.1. Seismic Data

[12] The major uncertainties in the calculation of the seismic strain stand on the estimates of the scalar moment M_0 of the earthquakes, which is directly related to the seismic part of the strain [*Kostrov*, 1974]. An additional uncertainty arises because the relationship between magnitude and seismic moment exhibits regional variations [*Ekström and Dziewonski*, 1988]. In particular, it appears that the Aegean region may yield somewhat higher M_s values than predicted from a global $M_s - M_0$ relation [*Ambraseys and Jackson*, 1990]. The global relations are likely, if anything, to overestimate the moments and hence the strain, which does not affect our results, since we will use only the relative values of the strain rate, and not the absolute ones. A final uncertainty is how to treat earthquakes that have subcrustal focal depths. Those earthquakes do not contribute to the deformation of the upper seismogenic layer and should not be included in the strain analysis. However, it is not always possible to distinguish deep events for the preinstrumental period. Figure 3a portrays

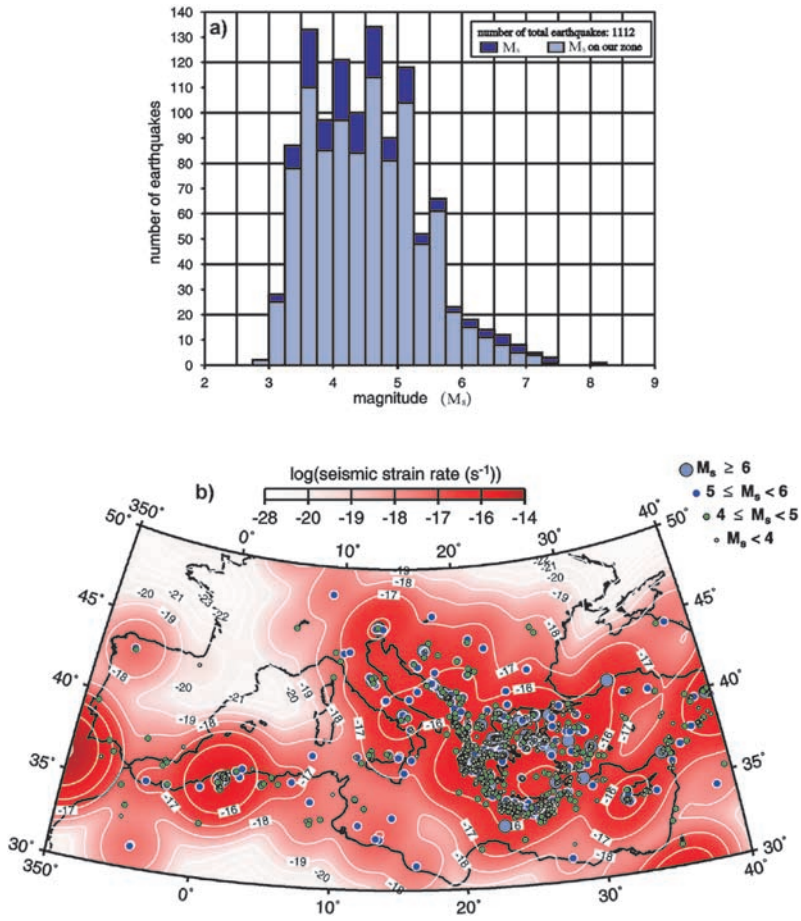

Figure 3. (a) Number of earthquakes as a function of the surface magnitude (M_s). The darkest histogram corresponds to all the earthquakes inside the area enlarged 5° of arc in each direction. (b) Seismicity with M_s (NEIC catalog, 1903–1999) and calculated seismic strain rate using the methodology described by *Kostrov* [1974].

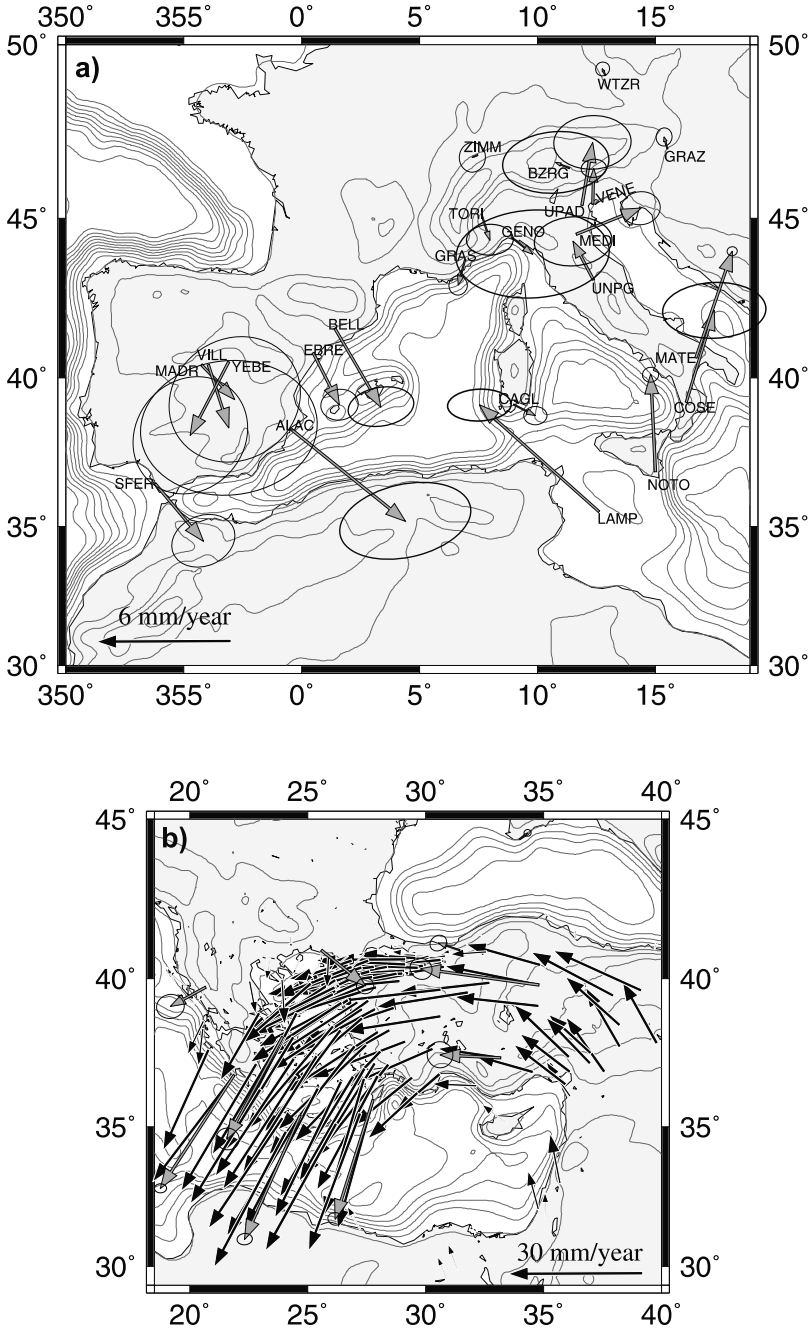

Figure 4. Geodetic data. Gray arrows have been obtained by the Matera Geodesy Center (CGS) [*Devoti et al.*, 2002], and black arrows by the GPS measurements made by *McClusky et al.* [2000] for (a) western Mediterranean and (b) eastern Mediterranean.

the number of earthquakes as a function of the magnitude M_s in the area under study, for magnitudes between 2.8 and 8. Figure 3b shows the geographical distribution of these events, superimposed on the seismic strain rates, in units of s^{-1}. We estimated the strain rate both including and excluding the apparently deep earthquakes within the studied area. The number and size of possible deep events are small, and their inclusion or exclusion makes no significant difference.

[13] We make use of the method explained by *Jiménez-Munt et al.* [2001a] to evaluate the seismic strain rate and to correlate it with that obtained from the numerical model. The seismic strain rate has been calculated using the methodology described by *Kostrov* [1974] which gives a measure of the brittle deformation according to

$$\dot{\epsilon} = \frac{1}{2\mu V \Delta t} \sum_{n=1}^{N} M_0^n, \tag{6}$$

where $\dot{\epsilon}$ is the strain rate, V is the deforming volume, μ is the shear modulus, and M_0^n is the seismic moment of the nth earthquake from the N total earthquakes occurring during the time interval Δt. Earthquake data have been compiled from the NEIC for the period between 1903 and 1999. The

seismic moment has been calculated according to *Ekström and Dziewonski* [1988], using the surface magnitude, M_s:

$$\log M_0 = \begin{cases} 19.24 + M_s & M_s < 5.3 \\ 30.2 - (92.45 - 11.4M_s)^{1/2} & 5.3 \le M_s \le 6.8 \\ 16.14 + \frac{3}{2}M_s & M_s > 6.8. \end{cases} \quad (7)$$

[14] To avoid border effects, we enlarged the study area by 5° in each direction, resulting in a total of 1112 seismic events with M_s between 2.8 and 8 (Figure 3). Finally, to calculate the seismic strain rate at each node of the grid, we assume that each earthquake involves a strain rate effect that follows a Gaussian function [*Jiménez-Munt et al.*, 2001a]. Several experiments have been performed in order to choose the most appropriate value for the Gaussian width in this area, which yield a value of 150 km. Figure 3b shows the resulting seismic strain rate and the epicenters of the earthquakes included in these calculations. The largest seismic strain rate release provided by equation (6) is of the order of $10^{-16} - 10^{-15}$ s^{-1}, occurring, from west to east, along the plate boundaries in north Africa, southern and northeastern Italy, along the Alps and Dinarides, in the Aegean region, and in western and eastern Anatolia. Except for a localized maximum in Algeria, this seismic strain rate pattern is characterized, owing to the combined effects of the real distribution of earthquakes and of the Gaussian distribution we have adopted, by a peculiar pattern portraying a region of $10^{-16} - 10^{-15}$ s^{-1}, embedding northeastern Italy, Dinarides, Aegean, and western Anatolia, surrounded by a region of lower strain rate release, of 10^{-17} s^{-1}. The pattern of Figure 3b agrees with that of the seismic moment rate density, in units of N m yr^{-1} m^{-2}, depicted in Figure 3 of *Ward* [1998], also based on the NEIC catalog.

[15] We define the strain rate correlation coefficient (SRC) between the logarithm of the seismic strain rate ($\dot{\epsilon}_{\text{seismic}}$) and the logarithm of the maximum absolute value between the three principal components of the strain rate calculated from the model ($\dot{\epsilon}$) as [*Jiménez-Munt et al.*, 2001a]

$$\text{SRC} = \frac{\sum_{i=1}^{N} [\log \dot{\epsilon}_i - \overline{\log(\dot{\epsilon})}][\log(\dot{\epsilon}_{\text{seismic}})_i - \overline{\log(\dot{\epsilon}_{\text{seismic}})}]}{\{[\sum_{i=1}^{N} (\log \dot{\epsilon}_i - \overline{\log(\dot{\epsilon})})^2][\sum_{i=1}^{N} (\log(\dot{\epsilon}_{\text{seismic}})_i - \overline{\log(\dot{\epsilon}_{\text{seismic}})})^2]\}^{1/2}}, \quad (8)$$

where N is the number of nodes of the grid and the overbar denotes the average value of the function over the modeled region. SRC takes values between −1 and 1, and its variability, as a function of the model parameters, will be discussed in Figure 16 in section 5.2.3. SRC = 1 means a perfect correlation between the seismic strain rate and the model results.

4.2. Geodetic Data

[16] The geodetic data set contains 190 vector velocities (Figure 4) with respect to a fixed Eurasia. Thirty-three of these geodetic velocities (gray arrows in Figures 4a and 4b) have been obtained by the Matera Geodesy Center of the Italian Space Agency (ASI-CGS) using Global Positioning System (GPS), satellite laser ranging (SLR), and very long baseline interferometry (VLBI) data [*Devoti et al.*, 2002]. These data have been completed in the eastern Mediterranean with the GPS measurements for the period 1988–1997 carried out by *McClusky et al.* [2000] (black arrows, also referred to Eurasia). *Devoti et al.* [2002] provide a detailed description of how the different GPS, SLR, and VLBI techniques have been combined in order to obtain reliable velocities for each site. In particular, the ASI-CGS solution in Figures 4a and 4b represents the residual velocity with respect to the Eurasian block obtained by subtracting the rigid motion of Eurasia expressed in the NUVEL-1A reference frame. The large error ellipses in the western and central Mediterranean (Figure 4a), especially in the Iberian peninsula and in northern sector of the Adriatic plate, indicate that geodetic data are still sparse and highly variable in these areas. In the eastern Mediterranean, error ellipses are provided only for the ASI-CGS solution, since the complete covariance matrix is not available to us for the *McClusky et al.* [2000] solution.

[17] A major characteristic of Figures 4a and 4b, from west to east, is the three different styles for the direction of the horizontal velocity field: a generally south trending direction in the Iberian peninsula and Ligurian coast of Italy, a generally north trending direction for southern and peninsular Italy, with a rotation from NW to NNE from the Lampedusa island (LAMP), between Africa and Sicily, to Matera (MATE) through Calabria (COSE) (Figure 4a), and finally a rotation from NNW to SSW from eastern Anatolia to the southern Aegean. The NE direction in southern Italy agrees with the suggestion of the counterclockwise rotation of the Adriatic plate [*Ward*, 1994; *Anderson and Jackson*, 1987]. Besides the velocity direction, the geodetic pattern is also characterized by another major feature, involving the magnitude of the velocity, which shows a substantial increase from the west to the east and from the north to the south. Note that in central and northeast Italy the motion has a strong north component except in the Po plain, with the site MEDI showing a large east component. This anomaly is probably due to local tectonic effects, for example, thrusts associated with the buried Apenninic chain, or to the water table [*Zerbini et al.*, 2001]. Lampedusa, Sicily, and peninsular Italy, except its westernmost coastal area, thus show a dominant north trending component, in agreement with the major NUVEL-1A velocity component at these longitudes. Moving to the eastern Mediterranean, in Figure 4b, we can highlight high velocities, ~30 mm yr^{-1}, with SSW direction in the Aegean region and with west directed velocities in the Anatolian Peninsula. In Figure 4b, the velocity field shows the northward motion of the Arabian plate and the counterclockwise rotation of the central western Anatolia and southern Aegean. This rotation is bounded to the north by the NAF and its extension into the Aegean Sea. The scalar measure of the misfit in the predicted velocity that we have adopted to compare modeled (u, v) and geodetic (u^{obs}, v^{obs}) velocities is the root mean square (RMS) of the prediction model and the observable data. We define

$$\text{RMS} = \left[\sum_{i=1}^{190} (u_i - u_i^{\text{obs}})^2 + \sum (v_i - v_i^{\text{obs}})^2\right]^{1/2} / (u_i^2 + v_i^2)^{1/2}, \quad (9)$$

where i is summed over the total number of geodetic sites, with u, v denoting the horizontal velocity components in the

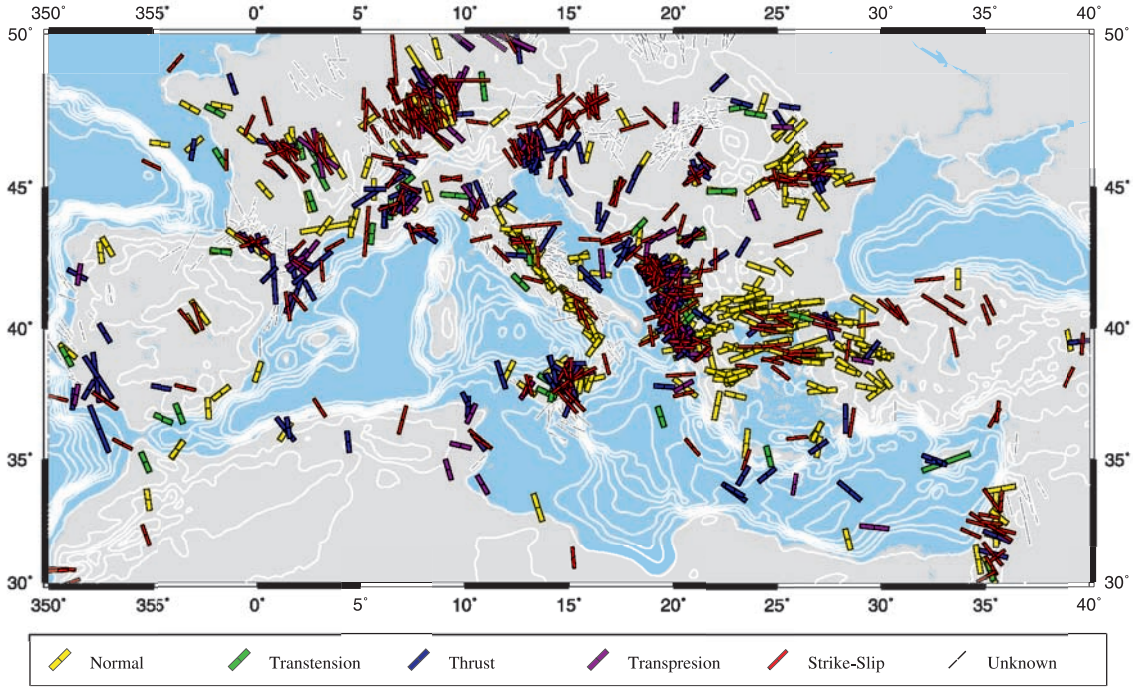

Figure 5. Directions of the most compressive horizontal principal stress from the World Stress Map project, WSM2000 [*Mueller et al.*, 2000]. The color of the symbol represents the tectonic regime, and its length is proportional to the quality of data.

longitudinal and latitudinal directions. In Figure 15 in section 5.2.3, the geodetic velocities will be used to calculate the principal horizontal strain rates, which can be compared with the modeled ones.

4.3. Stress Data

[18] Different categories of geophysical and geological data permit the determination of the approximate nature and orientation of tectonic stress acting on a given region. Most compressive horizontal principal stress orientations and local tectonic regimes have been compiled from the World Stress Map (WSM2000, *Mueller et al.* [2000]; Figure 5). They use different types of stress indicators, grouped into four categories: earthquakes focal mechanisms, well bore breakouts and drilling-induced fractures, in situ stress measurements, and young geological data. These different kinds of data generally show that one of the principal axes of the stress tensor is approximately vertical. Therefore the orientation of the stress is defined by specifying the azimuth of one of the horizontal principal stress axes. These data also include a quality coefficient describing the uncertainties associated to the stress orientation determination. We used 1384 principal stress direction of quality between A and C to compare with the directions predicted from the models.

[19] In the western Mediterranean, west of 10°E the maximum compressive horizontal stress is directed NNW, roughly parallel to the relative displacement between the European and African plates, except on arc structures such as the western Alps and Gibraltar Arc, where small stress deviations are observed. This contrasts with the central and eastern Mediterranean, where the stress field presents numerous deviations, localized within collision zones associated with large-scale faults and mountain belts as well as within active subduction zones (Calabrian and Hellenic Arcs).

[20] The tectonic regime along the plate boundary in north Africa and in a large part of Sicily reflects the convergence between Africa and Eurasia and shows a dominantly NW compressive trend. In the Calabrian Arc the stress regime is complex, diffuse in orientation and depth as well as in the style of deformation. According to *Rebaï et al.* [1992], the stress regime is close to radial extension. In the southern Apennines normal and strike-slip faulting prevail, with extension perpendicular to the chain [*Frepoli and Amato*, 2000]. In terms of tectonic regime, the northern Apenninic belt shows a clear distinction between an area of extension (the inner portion of the belt) and an area under horizontal compression or transpression along the Adriatic margin [*Ward*, 1994; *Frepoli and Amato*, 2000]. Northern Italy coincides with the Alpine orogenic belt and is mostly subject to a compressional regime [*Rebaï et al.*, 1992]. The state of stress changes from compressional in the east to extensional in the west, with radial extension localized within the southern part of the Aegean Sea. Particularly noticeable is the extension parallel to the hinge line of subduction in the Aegean. Within Anatolia, the stress direction undergoes a progressive counterclockwise rotation from a NE trending compression in the eastern Anatolia to a NE extension in the western Anatolia. This stress pattern is consistent with the westward movement of the Anatolian Peninsula. This peninsula is being pushed away from the collision zone along the north Anatolian right-lateral strike-slip fault (NAF) to the north, and the east Anatolian left-lateral fault (EAF) to the east [*Kahle et al.*, 2000]. It is also being pulled toward the Aegean by suction forces associated with the subduction. Extensional tectonics along the Aegean

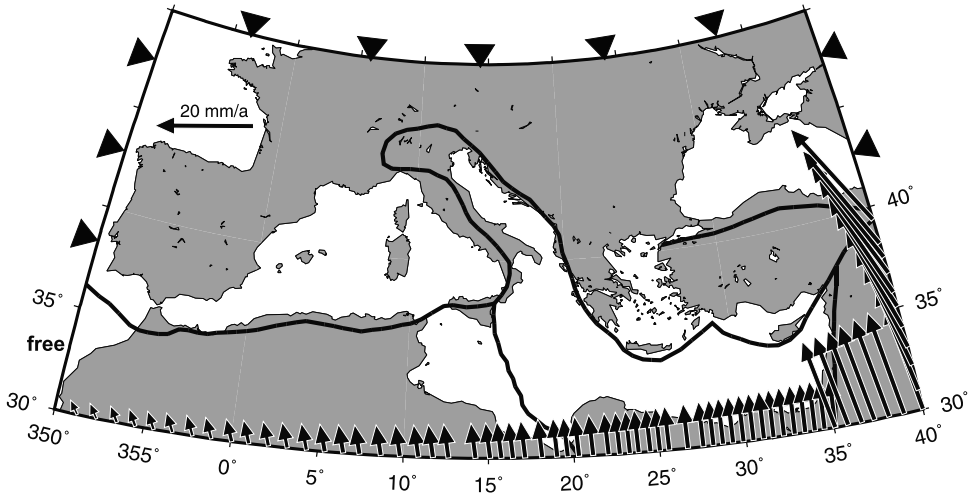

Figure 6. Boundary conditions corresponding to active convergence between Africa/Arabia and Eurasia plates, NUVEL-1A [*DeMets et al.*, 1994]. The thick black line represents the geometry of the considered weak zones.

back-arc basin suggests that the coupling between the African plate and the Anatolian block is weak [*Rebaï et al.*, 1992].

5. Results

5.1. Convergence Between Africa/Arabia and Eurasia

[21] We first attempt to reproduce the dynamics in the Mediterranean area by considering the active convergence between Africa/Arabia and Eurasia. The kinematics of these plates is governed by the counterclockwise rotation of Africa and Arabia relative to Eurasia. Several authors have constrained the relative velocity between these plates. We use the results of the global model of plate motion NUVEL-1A [*DeMets et al.*, 1994] to calculate the convergence between Africa and Eurasia and between Arabia and Eurasia (Figure 6). In this work we have assumed Eurasia as fixed, and the boundary conditions are taken relative to this plate. These include no motion of all Eurasian boundaries, namely, the northern boundary of the domain, the eastern boundary north of 40°N, and the western boundary north of 36°N. The southern boundary from 10°W to 35°E moves according to the Africa/Eurasia pole (located at 20.6°W and 21°N, with velocity of 0.12° Myr^{-1} [*DeMets et al.*, 1994]). As shown in Figure 6, the adoption of this Euler pole yields a velocity increasing from west to east, with 3.3 mm yr^{-1} in the direction of 35°W on the western most part and reaching around 10 mm yr^{-1} in the north direction near the Arabian boundary. The Arabian plate, southern boundary from 35°E to 40°E and eastern boundary south of 40°N, moves according to the Arabia/Eurasia pole (located at 13.7°W and 24.6°N, with velocity of 0.5° Myr^{-1} [*DeMets et al.*, 1994]). The Arabian velocities are between 20 and 24 mm yr^{-1}, varying their directions from south to north, from 10°W to 26°W.

[22] In this work, we have only considered majors faults, and we treat these by means of a continuous fault represented in the figures by a solid line, along north Africa, Calabrian Arc, Malta Escarpment [*Catalano et al.*, 2001], Apennines, Alps, Dinarides, Hellenic Arc, and Anatolian Faults. We tested different fault friction coefficients, from 0.85 to 0.01, where the friction coefficient of the continuum medium is fixed to 0.85. Figure 7 shows the maximum principal strain rate and velocity field driven by this active convergence. Figure 7a shows the results considering a plate boundary with the same friction coefficient of the continuum medium, that is 0.85. Figure 7b shows the case of a weaker plate boundary, with the friction coefficient lowered to 0.03. A coefficient of friction of 0.1 for the plate boundary means that it is about 1/5 as strong as the adjacent lithosphere, at equal strain rates.

[23] In the model with a fault friction coefficient of 0.85 (Figure 7a), the velocity due to the convergence diminishes gradually to the north. On average, the velocity is NNW trending in the African plate, while in the Eurasian plate it exhibits a major component to the west. In the center of Figure 7a the magnitude of the velocity changes from 8 mm yr^{-1}, at the latitude of 30°, to about 3–4 mm yr^{-1} at 45° latitude, in proximity of the Alps. Because of the increase to the east of the relative Africa-Eurasia relative motion, the largest horizontal velocities are attained in the easternmost part of the domain. It is interesting to note that the NAF and EAF accommodate the largest velocity variations that occur along the plate boundaries when convergence is the only active mechanism. In particular, they are larger than in the northern boundary of Africa and in the northernmost part of the Adria plate, along the Alps. The strain rate is concentrated along the plate boundaries, as expected, but it is higher in the aforementioned regions, namely, in north Africa, from Gibraltar to Sicily, along the Alpine front, and NAF, EAF. The resulting maximum deformation is in the eastern and western part of Eurasia and central Africa, with strain rates around 5×10^{-16} s^{-1}.

[24] The weaker plate boundary (Figure 7b) is responsible for a lower propagation, toward the Eurasian plate, of the velocity due to the active convergence. The velocity in the northern sector is drastically reduced with respect to Figure 7a. In the northernmost part of Adria, along the Alps, the velocity is reduced by a factor 3 with respect to Figure 7a to values of 1 mm yr^{-1} north of the Alps. The strain rate of the

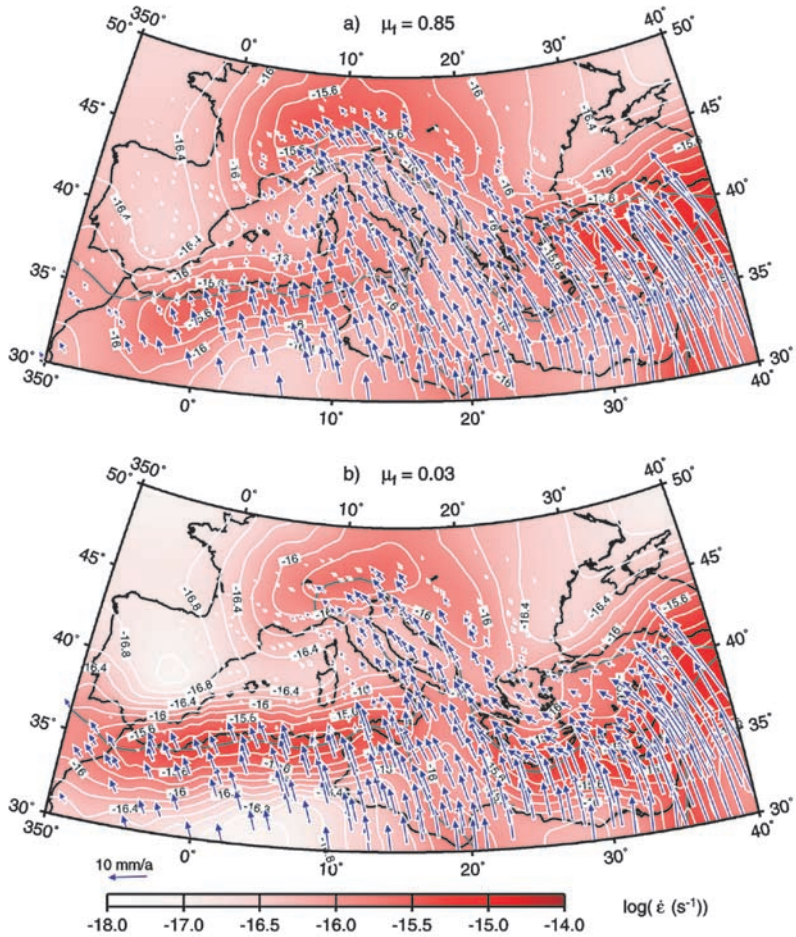

Figure 7. Maximum principal strain rate and velocity field driven by the active convergence (boundary conditions of Figure 6), with a friction coefficient on the plate boundary of (a) $\mu_f = 0.85$ and (b) $\mu_f = 0.03$.

order of 10^{-17} s^{-1} is reduced with respect to Figure 7a. The weaker north Anatolian Fault permits the westward motion of the Anatolian Peninsula. As in Figure 7a, the resulting highest deformation is concentrated along the plate boundary in north Africa, east of the Alps, and in the Anatolian peninsula. This contrasts with the low strain rates obtained in central Italy, where the plate boundary is practically parallel to the calculated velocity field. When comparison is made between Figures 4a and 4b, only the velocity field in north Africa, represented by the sites of Lampedusa and Noto, and in the easternmost part of Anatolia is correctly reproduced in magnitude, with some deviation in the direction; the modeled trend is NNW, while it is NW trending in the geodetic constraints. In northeast Italy, the magnitude of the velocity is correctly reproduced, while the observed one exhibits an eastern component that differs from the western one carried by the model. In central Italy, the velocity is well reproduced both in magnitude and direction, while in southern Italy, from Sicily to Matera, the modeled velocities do not show the characteristic rotation to the east. From Anatolia to the west to the Aegean, the model velocity is incorrect, both in magnitude and direction; the predicted rates are at most 10 mm yr^{-1}, in comparison with the 30 mm yr^{-1} observed in the Aegean, and north trending rather than south trending, in the Aegean and western Anatolia. Comparison with the seismic strain rate of Figure 3b confirms the results of the geodetic velocity analysis that convergence accounts solely for the seismic strain rate in north Africa, northern Italy, and eastern Anatolia. The large strain rates in southern Italy and in the Aegean Arc do not appear in Figures 7a and 7b. In both Figures 7a and 7b, minor strain rate accumulation occurs along the remaining plate boundaries, in particular, along the Malta escarpment and SAF, in the Aegean, and in the Italian peninsula. The regions that are essentially unaffected by the strain accumulation are in the Iberian peninsula, in the northeast part of the studied domain, and in Africa, at 30°N latitude, from 0° to 10°E longitude. Strain rates vary in the range $10^{-16.4}$ s^{-1} in the slowly deforming regions, up to 10^{-15} s^{-1} in eastern Anatolia. This model, in which convergence is the only active mechanism, is not able to reproduce the geodetic velocity and the large strain rate accumulation observed in the south of Italy and in the Aegean region.

5.2. Convergence and Subduction Forces

[25] In order to improve the correlation between modeled results and the geodetic velocities and seismic strain rates, we now make use of another family of models that includes the effects of subduction in the Aegean (Hellenic Arc) and

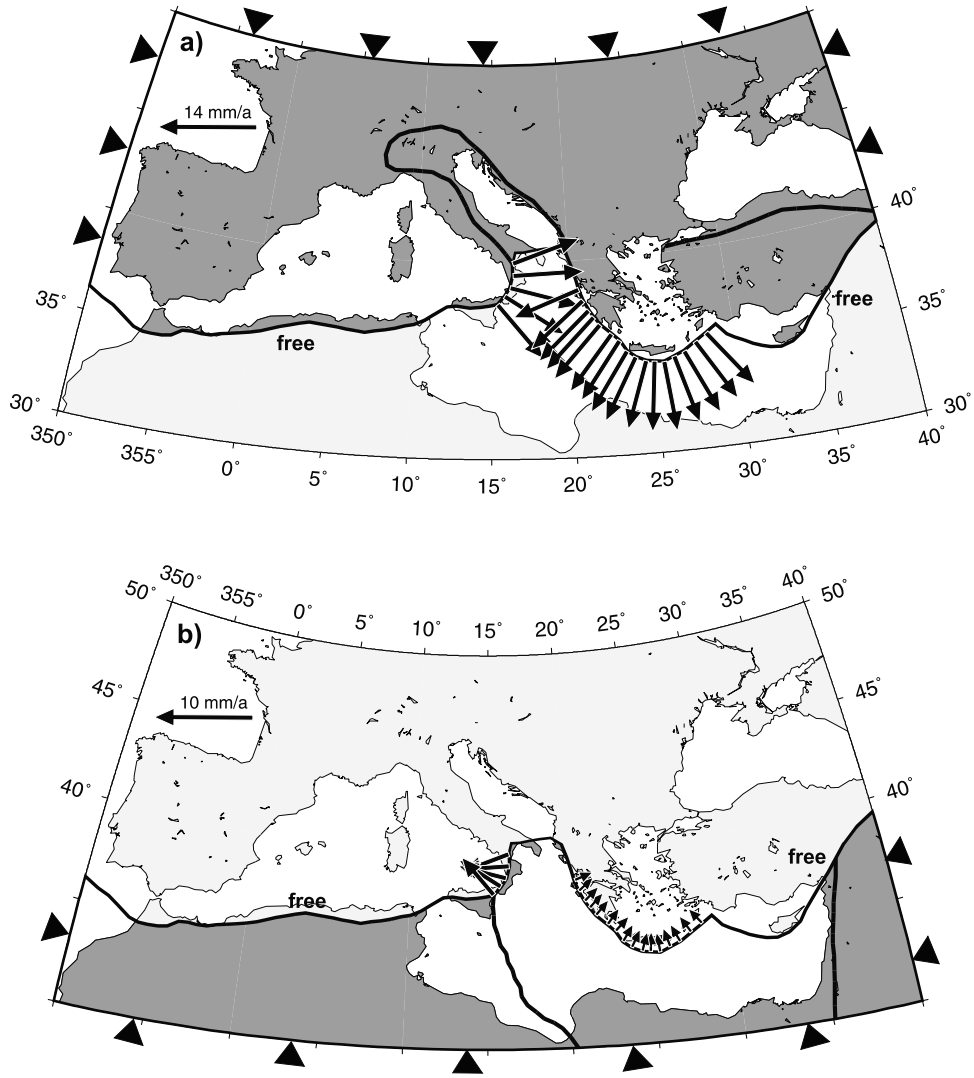

Figure 8. Boundary conditions corresponding to the subduction forces. (a) North model, velocities due to the suction force applied at the overriding plate, Tyrrhenian and Aegean Sea. (b) South model, velocities due to the slab pull applied at the subducting plate.

southern Italy (Calabrian Arc). Within a thin-plate formulation, this can be achieved by applying the appropriate horizontal velocities at the plate boundaries that simulate the effects of tectonic forces due to trench suction on the overriding plate and slab pull on the subducting plate [*Bassi et al.*, 1997; *Meijer and Wortel*, 1996]. This implies that the plate boundary must coincide with a boundary of the model. We thus divide the model along the plate boundary and consider separately the Eurasian plate and the African plate (Figure 8). In this way, we can apply the appropriate velocity boundary conditions where subductions are active.

[26] From subduction models in vertical cross sections [*Giunchi et al.*, 1996a] or 3-D models [*Negredo et al.*, 1997, 1999], where the effects of trench suction and slab pull are taken self-consistently into account, we estimate the horizontal velocities that should be applied along the trench regions to simulate the effects of subduction. These velocities are portrayed by the black arrows perpendicular to the arcs for the Eurasian plate (Figure 8a) and Africa plate (Figure 8b). We have verified that the velocity boundary conditions that we have applied yield suction and slab pull forces that agree, in magnitude, with the tectonic forces applied by *Meijer and Wortel* [1992] to simulate the effects of subduction in the Andes.

[27] The remaining plate boundaries (north Africa and eastern Anatolia), where subduction is not presently occurring, are subject to free boundary conditions, where the only effects are those to due the lithostatic stress. Our approach is appropriate under the assumption that the horizontal velocities induced by subductions are negligible along these (nonsubducting) plate boundaries relative to the horizontal velocities induced by Africa-Eurasia and Arabia-Eurasia convergence along the same boundaries. The validity of this assumption has been verified a posteriori by checking the size of the velocity induced along these plate boundaries by the subduction activated on the Calabrian and Hellenic Arcs, with respect to the velocity field induced by convergence.

5.2.1. Model A

[28] For the Calabrian Arc we make use of the horizontal velocities obtained by means of previous 2-D dynamic models in the Tyrrhenian Sea [see *Giunchi et al.*, 1996a, Figure 4b]. We thus have 10 mm yr^{-1} applied at the edge of

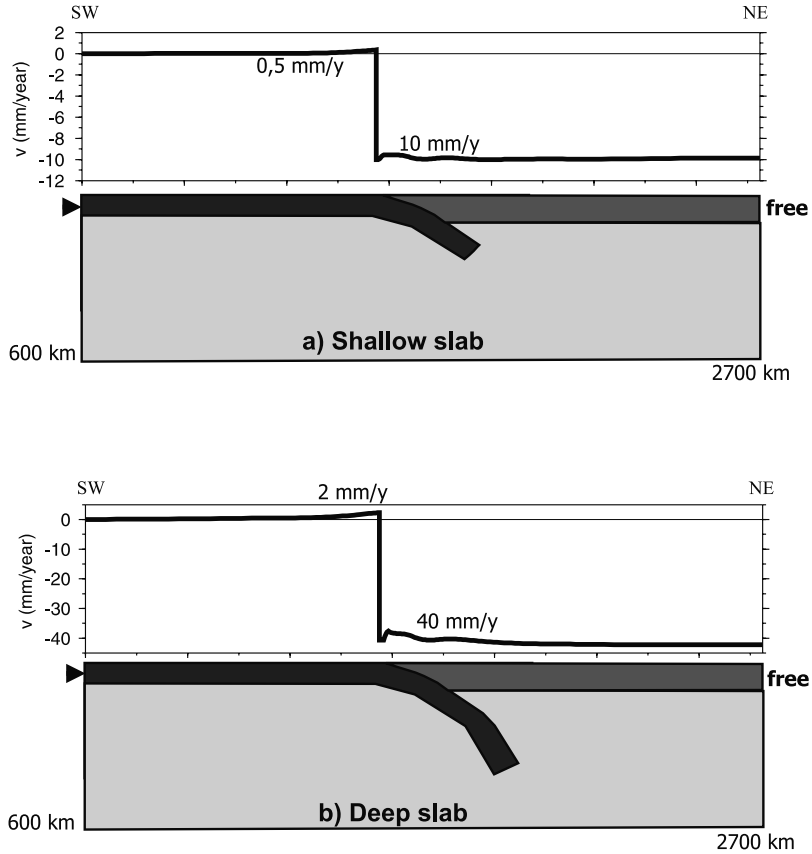

Figure 9. Geometry of the 2-D subduction models representative of the Hellenic subduction and resultant surface horizontal velocities. Positive values correspond to NE directed velocities, while negative ones correspond to SW velocities. (a) Shallow slab, inferred from the seismicity distribution, velocities used in model A. (b) Deep slab, inferred from the tomography, velocities used in models B and C.

the overriding plate (Eurasia) along the arc and 5 mm yr^{-1} at the edge of the subducting plate (Africa). These velocities are applied perpendicularly to the arc in Figures 8a and 8b for the overriding and underthrusting plates, respectively.

[29] For the Hellenic Arc a new series of 2-D subduction models, in vertical cross section, has been implemented to calculate the horizontal velocities resulting from slab pull and suction forces (Figure 9). The cartoons shown in Figure 9 are representative of a profile perpendicular to the Hellenic Arc, approximately in the NE direction. To evaluate the slab pull effects, positive density contrasts, based on the petrological studies of *Irifune and Ringwood* [1987], are assigned to the subducting crust and harzburgite when they exceed the depth of about 90 km. In Table 2 we specify the parameters defining the viscoelastic subduction models. The term "elapsed time" denotes the time interval after the activation of the density contrasts at the subduction zones when steady state horizontal velocities are obtained at the hinge line of the subduction. These models are purely gravitational, driven solely by the negative buoyancy sub-

Table 2. Characteristics of the Hellenic Arc Models Shown in Figure 9

	Rheology			
	Viscosity η, Pa s	Poisson's Ratio ν	Young's Modulus E, Pa	Geometry Thickness, km
Subducting crust + harzburgite	10^{24}	0.27	1.75×10^{11}	20 + 20
Subducting lithosphere mantle	5×10^{22}	0.27	1.75×10^{11}	40
Overriding crust	10^{24}	0.25	9×10^{10}	30
Overriding lithosphere mantle	5×10^{22}	0.27	1.75×10^{11}	70
Upper asthenosphere mantle	10^{21}	0.27	1.75×10^{11}	500
Lower asthenosphere mantle	3×10^{22}	0.27	1.75×10^{11}	1200

Other Characteristics	Value
Model width × Model depth	2700 km × 1800 km
Slab thickness × Slab depth	
Model A	80 km × 180km
Models B and C	80 km × 400 km
Elapsed time	250 kyr

ducted portion of the slab. The distribution of earthquakes [*Kiratzi and Papazachos*, 1995; *Papazachos et al.*, 2000] suggests a slab reaching a depth of about 180 km, partitioned into two parts, a shallow one with a lower dipping zone and a steeper one between 100 and 180 km.

[30] We have verified that rollback is extremely sensitive to the boundary conditions and to the geometry of the slab. The horizontal velocity of the subducting plate is fixed at the SW boundary, while a free boundary condition is applied at the opposite edge of the overriding plate. The fixed boundary conditions at the left edge of the subducting plate allow us to evaluate the relative velocities of the two plates at the hinge line with respect to the subducting plate. The free boundary conditions at the right edge of the overriding plate account for the possibility that the Anatolian block moves freely toward the subduction zone. This movement is a consequence of the suction force exerted by the negatively buoyant subducting plate and of the independent motion of Anatolia with respect to Eurasia and Africa. Once the relative velocities due to subduction have been evaluated at the hinge line, they can be applied to the Eurasian and African plates, as shown in Figures 8a and 8b, in order to retrieve the velocity field induced by subduction that must be added to the velocity due to convergence.

[31] Our first model (Figure 9a) takes into account only the seismically active part of the Aegean slab. Under these conditions, the velocity obtained at the edge of the subducting plate (Africa) in the arc due to slab pull is 0.5 mm yr^{-1} and the velocity of the overriding plate (Eurasia) at the contact between the subducting and overriding plate is 10 mm yr^{-1}. We consider these velocities as boundary condition for the Aegean border in the thin-sheet model. Once the velocities due to convergence and subduction are summed up, the relative velocities between the plates along the plate boundary account self-consistently for both the effects of the relative large scale motion of Africa/Arabia with respect to Eurasia and the effects of the gravitational forces at the subduction zones. Our thin-sheet modeling for the Aegean subduction is thus consistent with geodynamic models that have been proposed to explain widespread extension in the Aegean. Generally, these models emphasize either the westward motion of the Anatolian block [*Dewey and Sengor*, 1979; *Taymaz et al.*, 1991] or the occurrence of rollback of the South Hellenic subduction [*Le Pichon and Angelier*, 1979; *Wortel and Spakman*, 2000].

[32] Figures 10 and 11 show the resulting velocities and strain rate driven by active convergence and trench suction and slab pull in the Aegean Sea, for the shallow subduction of Figure 9a, and in the Tyrrhenian Sea. The gray and black arrows denote the observed data and model results, respectively. In Figure 10 we obtain an improvement in fit to the velocity measured in southern Italy and a global agreement with the SW recorded geodetic data in the Aegean area. In southern Italy the model fails to reproduce the smooth west to east rotation of the geodetic velocity, with the site in the Calabrian Arc modeled with a too large eastward component. With respect to Figure 8, this eastward component is due to the outward velocity applied to the arc on the overriding plate that is intended to simulate suction effects due to subduction. As expected, the effects of subduction are not felt in northern Italy. In Figure 10b the velocities predicted from the model show the counterclockwise rotation from Anatolia to the Hellenic Arc, although these velocities are nearly 4 times smaller than the observed velocities in the Aegean; these results thus show the contribution of push forces from the Arabian plate and of the shallow subduction to the westward extrusion of Anatolia. These mechanisms induce, with respect to Figure 7b, a rotation in the modeled velocity from NW to SW, in closer agreement with the data. It is noticeable that the magnitude of the velocity is lower than the observed one in the whole Aegean. A severe mismatch also occurs in the center of Anatolia, both in direction and magnitude, while in the easternmost Anatolia, the modeled velocity agrees with the data, indicating the reasonableness of the boundary conditions for the velocity of the Arabian plate adopted in the modeling.

[33] Figure 11 shows the modeled maximum principal strain rate in the Eurasia and Africa/Arabia plates. The highest strain rate occurs in the Aegean region, along the East Anatolian Fault, in southern Italy, and along the plate boundary in north Africa, which is well correlated with the highest seismicity. The effect of subduction is to increase the strain rate in the subduction zones, yielding strain rates in the Hellenic Arc of around 10^{-15} s^{-1}. The modeled strain rate of Figure 11 can be compared with the seismic one of Figure 3b. In comparison to the case in which convergence is the only active mechanism, the inclusion of subduction significantly improves the fit to the strain rate pattern from southern Italy to eastern Anatolia, through the whole Aegean region. In general the pattern of maximum release of seismic energy is also well reproduced. The modeled intensity of the strain rate is generally higher than the seismic one, in agreement with the expectation that the strain is not released solely by earthquakes but also via ductile viscous creeping. The $10^{-15.6}$ s^{-1} isoline encircling southern Italy, the Aegean and western Anatolia, fits well with the 10^{-16} s^{-1} isoline contouring the same regions in Figure 3b. Except for central Italy, the earthquakes fall within the red region where the modeled strain rate is the largest, from Gibraltar, through southern Italy, the Alpine front, Dinarides, the Aegean to Anatolia. This reconciliation of the real earthquake distribution indicates that the major tectonic mechanisms in the Mediterranean have been properly taken into account, except in central Italy, where our model does not include any extra mechanisms except the motion of the Adriatic promontory induced by Africa-Eurasia convergence. Extension could be controlled by subduction underneath the Apennines. This subduction, which is poorly constrained, is not included in our study, which makes this part of peninsular Italy different from the Calabrian and Hellenic Arcs.

5.2.2. Model B

[34] Different studies assume a deeper slab below the Aegean, relative to Figure 9a, with the slab penetrating into the lower mantle, dipping at higher angle, down to 600 km [*Jonge et al.*, 1994; *Bijwaard et al.*, 1998; *Wortel and Spakman*, 2000]. Some tomographic models showed signs of slab detachment between 100 and 200 km below the westernmost part [*Spakman et al.*, 1993], whereas others did not [*Piromallo and Morelli*, 1997]. However, in all models a continuous slab is observed below the central and western part of the Hellenic Arc. According to the tomography a second thin-sheet model (model B) uses the velocities obtained with a deeper slab in the 2-D Hellenic subduction simulation. In fact, we have considered a deeper slab,

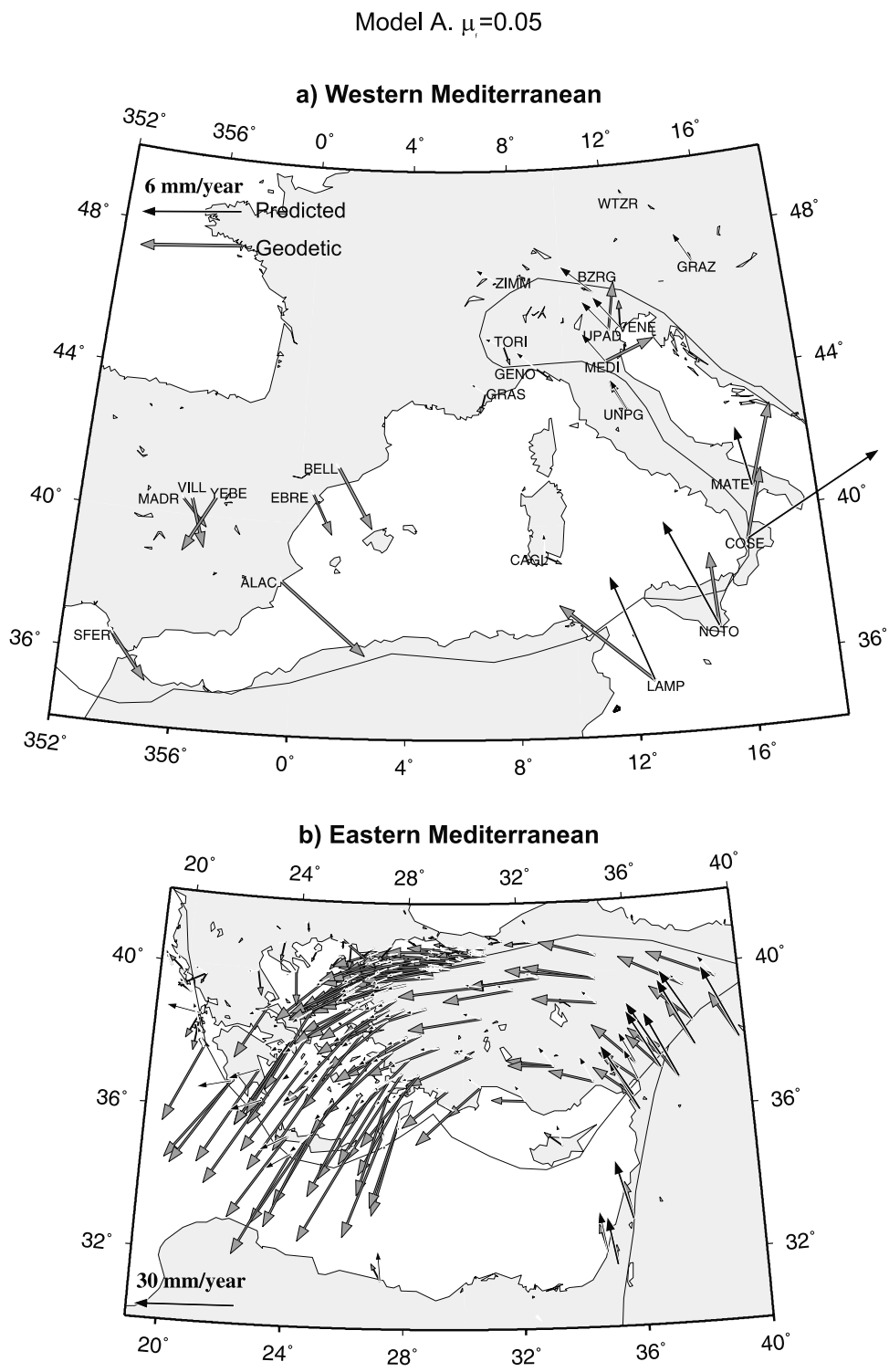

Figure 10. Geodetic and predicted velocities resulting from model A, with both effects, the active convergence and subduction forces in the Aegean and Tyrrhenian Sea, considering a shallow slab in the Hellenic Arc for (a) western Mediterranean and (b) eastern Mediterranean. Gray arrows denote the geodetic data, and solid arrows denote the predictions from the model.

dipping with a higher angle between 200 and 400 km (Figure 9b). We use the same density contrast as a function of depth as *Giunchi et al.* [1996a], based on the petrological model of *Irifune and Ringwood* [1987]. With the same boundary conditions as in the shallower slab model, the resulting velocities are 2 mm yr^{-1} for the subducting plate and 40 mm yr^{-1} for the overriding one (Figure 9b).

[35] Figures 12 and 13 show the results of the thin-sheet model B obtained by summing the effects of the Aegean deeper slab, Calabrian subduction, and Africa/Arabia and

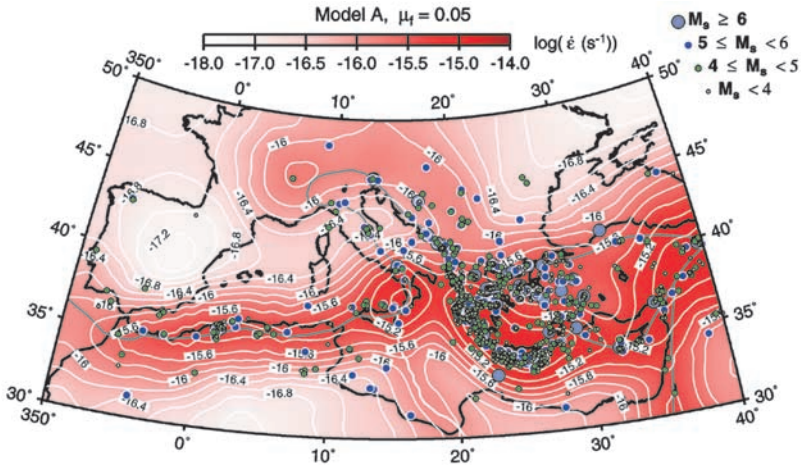

Figure 11. Maximum principal strain rate resulting from model A, with both effects, the active convergence and subduction forces in the Aegean and Tyrrhenian Sea, considering a shallow slab in the Hellenic Arc. The seismicity is represented with the colored dots, where the dot dimension is proportional to the magnitude.

Eurasia convergence. Figure 12 depicts the geodetic and predicted velocities, and Figure 13 depicts the modeled maximum principal strain rate. With respect to Figures 10a and 10b, we notice minor deviations in the modeled velocities in southern Italy due to the relatively large distance of the Aegean Arc (see Figure 8b) and a substantial improvement in Figure 12b with respect to Figure 10b. The agreement with the geodetic data in the Aegean region is substantially improved (Figure 12b). The model yields westward motion of the central Anatolia with velocities between 10 and 20 mm yr^{-1}, thus improving the velocity pattern in this region with respect to Figure 10b, and the counterclockwise rotation of these velocities toward SSW in the Hellenic Arc, with velocities of 35–40 mm yr^{-1}. However, the predicted velocities at the edges of the Hellenic Arc, as well as in the Calabrian Arc, are higher than the geodetic ones. The highest strain rate (Figure 13) occurs along the plate boundary, in north Africa, southern Italy, Aegean region, and Anatolia. In these cases, the values in the Aegean Sea are higher, with a maximum achieved in the Hellenic Arc ($\sim 10^{-14.6}$ s^{-1}). The predicted relative minimum of the strain rate between western and eastern Anatolia fits remarkably well the observed seismic strain rate pattern (Figure 3b).

5.2.3. Model C

[36] As discussed above, the modeled velocity in the Calabrian Arc and at the edges of the Hellenic Arc results is higher than the geodetic velocities. We will show that this effect results by assuming velocities which are uniform along the hinge of subduction. We can overcome this shortcoming of the modeling using results obtained within 3-D dynamic models of subduction [see *Negredo et al.*, 1997, Figure 3a, dotted line]. This study modeled the variation of horizontal velocities in the Tyrrhenian and Adria-Ionian domains along the subduction hinge line, when only subduction is modeled. In the southern Calabrian Arc the maximum velocity of the overriding plate (Tyrrhenian) predicted from the 3-D model is 3.5 mm yr^{-1} toward the Ionian Sea, while the subducting plate moves toward the Tyrrhenian Sea at 1 mm yr^{-1} due to the slab pull. These values decrease from south to north along the hinge line because of the finite extension of the subducted plate. We use these velocities in our thin-shell model, imposed at the plate boundary in the Calabrian Arc, to simulate the suction force and the slab pull for a laterally varying subducted lithosphere. We also consider a similar decrease of the velocity from the center of the Hellenic Arc to its lateral edges.

[37] Figure 14 compares the velocities predicted under these new conditions and the geodetic data. We observe that in the Calabrian Arc the modeled and the observed velocity are well matched, with Matera (MATE) unaffected by the more realistic velocity conditions. The velocities at the edges of the Hellenic Arc are reduced with respect to Figure 12b, as is the misfit in orientation. With respect to Figures 10b and 12b we note a better fit of the velocities in the southern part of Anatolia and Ciprus Island, with some disagreement in northern Anatolia, in the velocity magnitude. In fact, the modeled velocity is 9–14 mm yr^{-1}, to be compared with the observed values of 17–22 mm yr^{-1}. North of the NAF, we note a drastic decrease in both modeled and observed velocities, indicating that this fault represents a strong discontinuity of the lithosphere. The smoother northward decrease in the velocity modulus of the model, when compared with the geodetic velocity, indicates that our continuous rheological model is not fully capturing the Anatolia's block-like behavior. As observed by *McClusky et al.* [2000], the intrablock velocity pattern, resulting from observations and modeling, is thus coherent with the rotation of the blocks in the eastern Mediterranean. This block-like behavior of Anatoia is also visible in the relative minimum of the strain rate, observed in the seismicity (Figure 3b) and predicted by the model (Figure 13). A detailed study is done by *Jiménez-Munt and Sadadini* [2002].

[38] Figure 15 portrays the eigenvectors and eigenvalues of the modeled and geodetic strain rate tensor. The western, central, and eastern Mediterranean (Figures 15a–15d) have been subdivided into triangles with vertices connecting the sites where the horizontal velocity components are available. The aim is to estimate the strain rate, from the numerical and geodetic standpoint, indicative of the style of deformation in the area within each triangle. In our

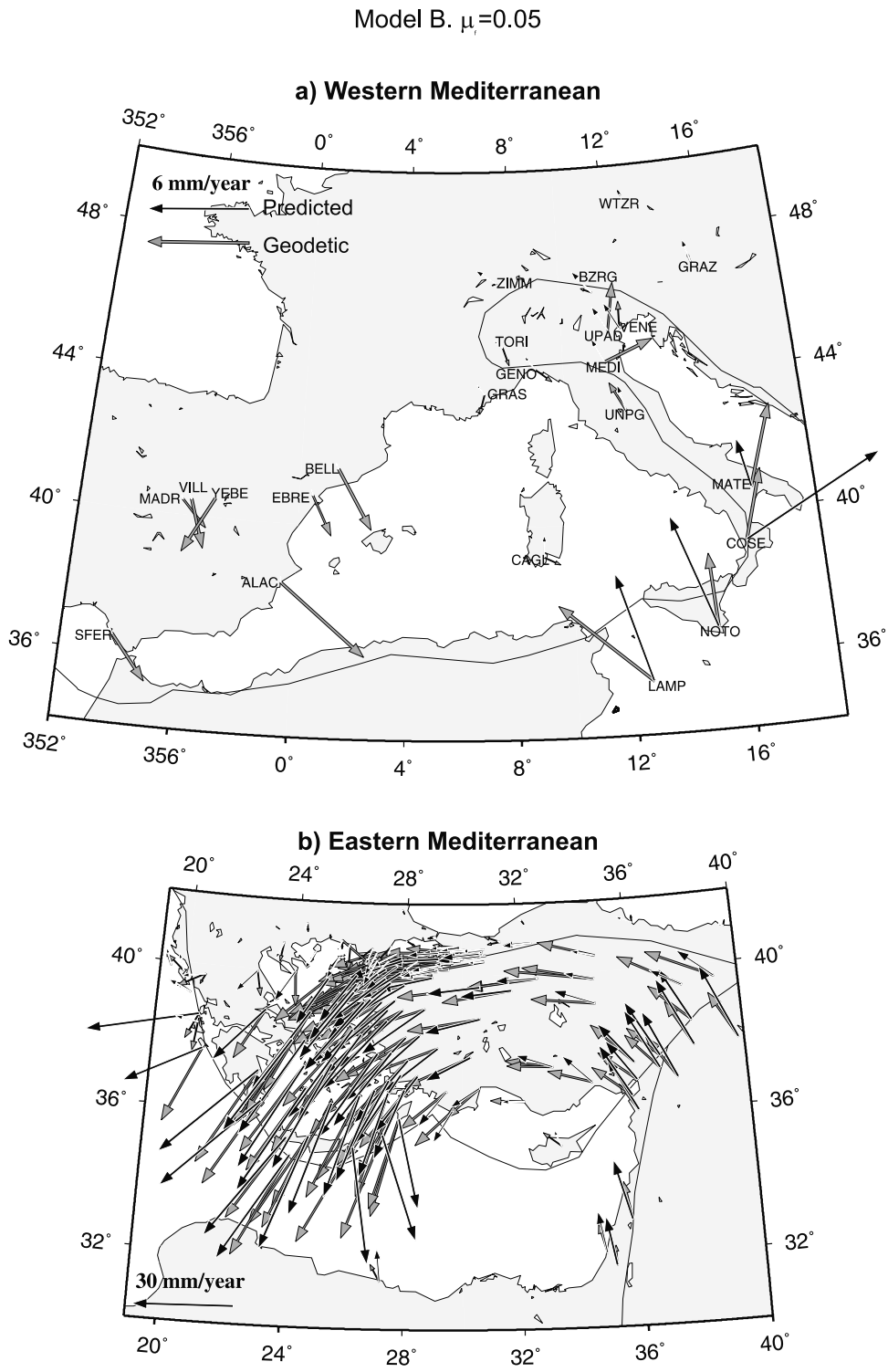

Figure 12. Geodetic and predicted velocities resulting from model B, with the active convergence and subduction forces in the Aegean and Tyrrhenian Sea, with a deep slab in the Hellenic subduction for (a) western Mediterranean and (b) eastern Mediterranean. Gray arrows denote the geodetic data, and solid arrows denote the predictions from the model.

approach, this is accomplished assuming that the horizontal velocity components vary linearly with distance within each triangle. This constant space gradient provides a first order approximation of the strain rate in each tectonic region embedded within the vertices of the triangles. This approximation can be improved by integrating the geodetic network with new geodetic sites. We have elected the bisectors of each triangles as the reference point where the strain rate tensor is evaluated. The same procedure, described in detail by *Devoti et al.* [2002], is applied to the two series of

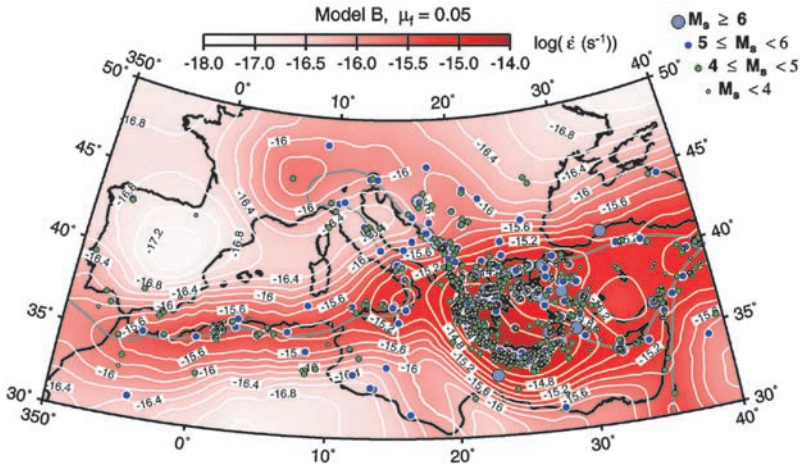

Figure 13. Maximum principal strain rate resulting from model B, with the active convergence and subduction forces in the Aegean and Tyrrhenian Sea, with a deep slab in the Hellenic subduction. The seismicity is represented by the colored dots, where the dot dimension is proportional to the magnitude.

horizontal velocity components, the geodetic and the modeled ones. In dealing with the known velocity positions at the vertices of the triangles, the solution requires the inversion of a system of linear equations in six unknowns: four tensor components plus two velocity components at the reference point. The velocity gradient tensor can then be decomposed into its symmetric part and antisymmetric part, the first one providing the strain rate eigenvectors and eigenvalues, after the diagonalization procedure, while the second one provides a rigid rotation rate. The errors associated with the geodetic strain rate tensor are obtained by means of the covariance matrix associated with the velocity components at each site. In Figure 15, the eigendirections are given by two perpendicular arrows, oriented with respect to the meridian; the length of the arrow is scaled to provide the eigenvalue in units of 10^{-9} yr^{-1}. Red stands for compression and black for extension, with arrows in bold representing the geodetic strain rate and the empty arrows the numerically retrieved strain rate, on the basis of the last model C. From west to east, we now compare the geodetically retrieved strain rate tensor with the numerical one and with the stress map WSM2000 of Figure 5.

[39] In the western Mediterranean (Figure 15a), SFER-ALAC-CAGL-LAMP, compression predominates in the NNW direction. The eigendirection relative to this compression is well reproduced by the model, between 5°W and 10°E longitude. This is particularly true within the triangle SFER-ALAC-LAMP, where the geodetic and modeled eigendirections agree within the standard deviation σ, represented by the gray surface surrounding the eigenvectors of the geodetic strain tensor. In the same triangle, the modeled eigenvalue is a factor two lower than the geodetic one, indicating that the model underestimates the compression. This eigenvalue is well reproduced in the central Mediterranean, in the triangle ALAC-CAGL-LAMP. The NNW compression in the western Mediterranean is in good agreement with the observed stress data (Figure 5), as indicated by the thrust events (blue bars) in north Africa and in the western part of Sicily. This compression is consistent with the view that it is induced by the relative motion between Africa and Eurasia [*DeMets et al.*, 1994]. South of LAMP, the geodetic compression rotates by 90° with respect to the western Mediterranean, but this compression is not reproduced by the model and the large accompanying extension is severely underestimated. In the region from LAMP to MATE, the ENE compression is now well reproduced by the model. The north trending extension is underestimated in the modeling, except for the triangle with vertices in LAMP and NOTO, where we obtain the best fit, as far as the magnitude of compression and extension is concerned. The change in strain style from LAMP to the northeast is evident in the stress data, where from the eastern part of Sicily to the Calabrian Arc we notice a change from thrust (compression) to normal faults events (extension). This change is particularly well reproduced by the geodetic strain rate and to a lesser extent by the modeling. A wide zone of strike-slip events in WSM2000 well correlates with the 90° rotation in the eigendirection from west to the east with respect to LAMP. In the Iberian peninsula, modeling and observation are in complete disagreement. This negative result seems to indicate that some major tectonic features are not modeled in the westernmost part of the studied domain or that the quality of the geodetic data is presently insufficient. At the light of geological and geophysical observations, several competing models have been proposed to explain the geodynamic evolution of the region. These models include escape tectonics, subduction and slab retreat, lithosphere-mantle delamination, orogenic collapse, etc. [e.g., *Platt and Vissers*, 1989; *Royden*, 1993; *Zeck*, 1996; *Seber et al.*, 1996; *Marotta et al.*, 1999]. Up to now, however, there has been no consensus among the possible active mechanisms, since their numerical modeling has produced results that are not coherent with observation. On other hand, the geodetic data in the westernmost Mediterranean appear to be insufficient in terms of both geographical distribution and length of the acquisition time to allow to discriminate among the various tectonic hypotheses.

[40] The eigendirections of the modeled and geodetic strain rate are best reproduced in the western part, with underestimated dominant compression. In the eastern part of the study area the nature of the fit is different, with generally well reproduced eigenvalues but with some deviation between the eigendirections. The compression that rotates

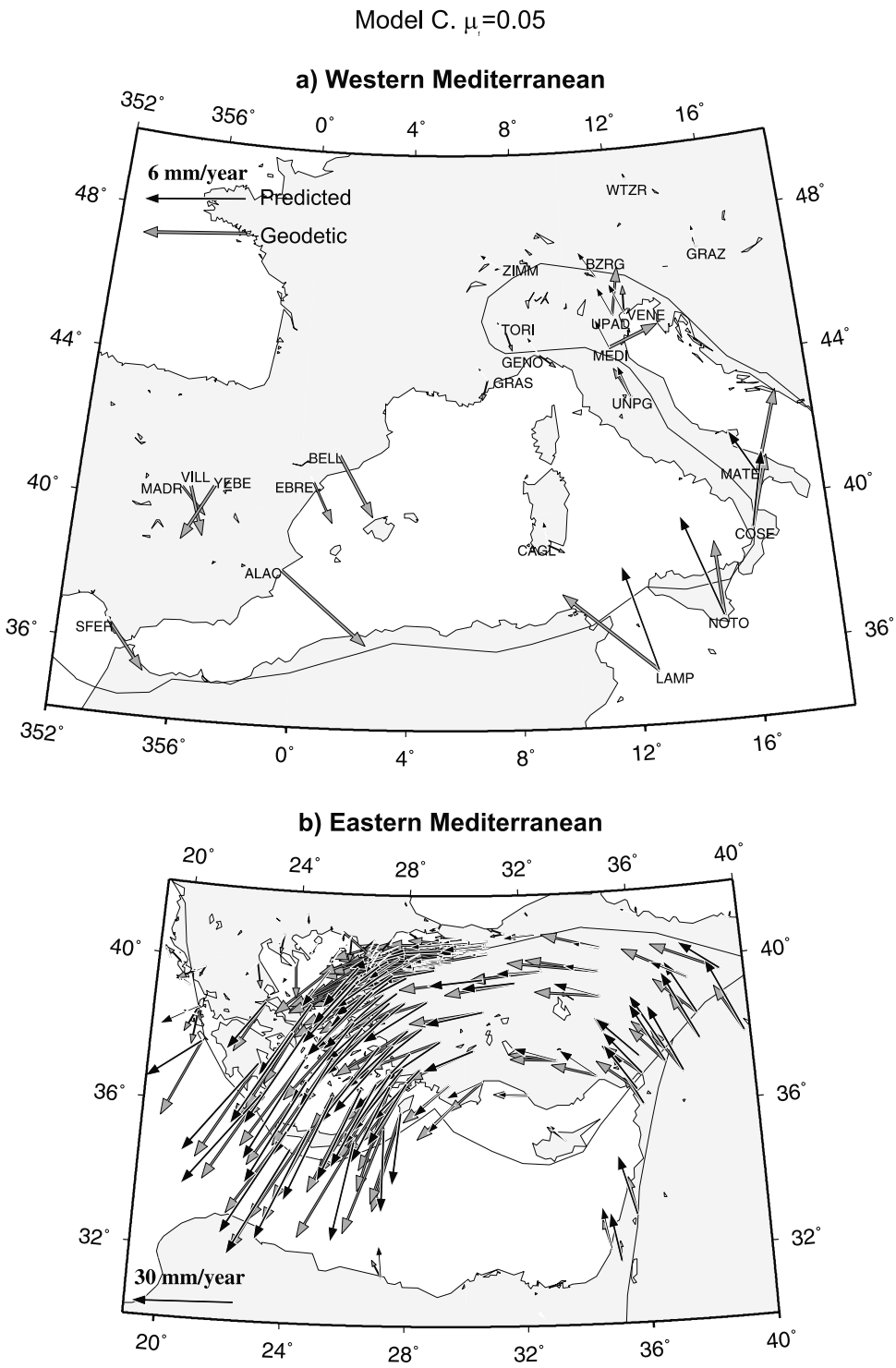

Figure 14. Geodetic and predicted velocities resulting from model C, with the active convergence and subduction forces in the Hellenic (deep slab) and Calabrian Arcs, decreasing the velocity from the center of the arc to the boundaries [*Negredo et al.*, 1997] for (a) western Mediterranean and (b) eastern Mediterranean. Gray arrows denote the geodetic data, and solid arrows denote the predictions from the model.

by 90° with respect to the western Mediterranean, leading to a compression which is roughly perpendicular to the arc, seems to be a surface fingerprint of subduction.

[41] In the center of the Tyrrhenian Sea (Figure 15b), CAGL-UNPG-NOTO and NOTO-UNPG-COSE, the geodetic and the model strain rates are in close agreement, both in the eigendirections and eigenvalues. In proximity to this region, UNPG-MATE-COSE portrays the worst fit, with the modeled compression aligned with the geodetic extension, due to the mismatch, already noted, between the modeled

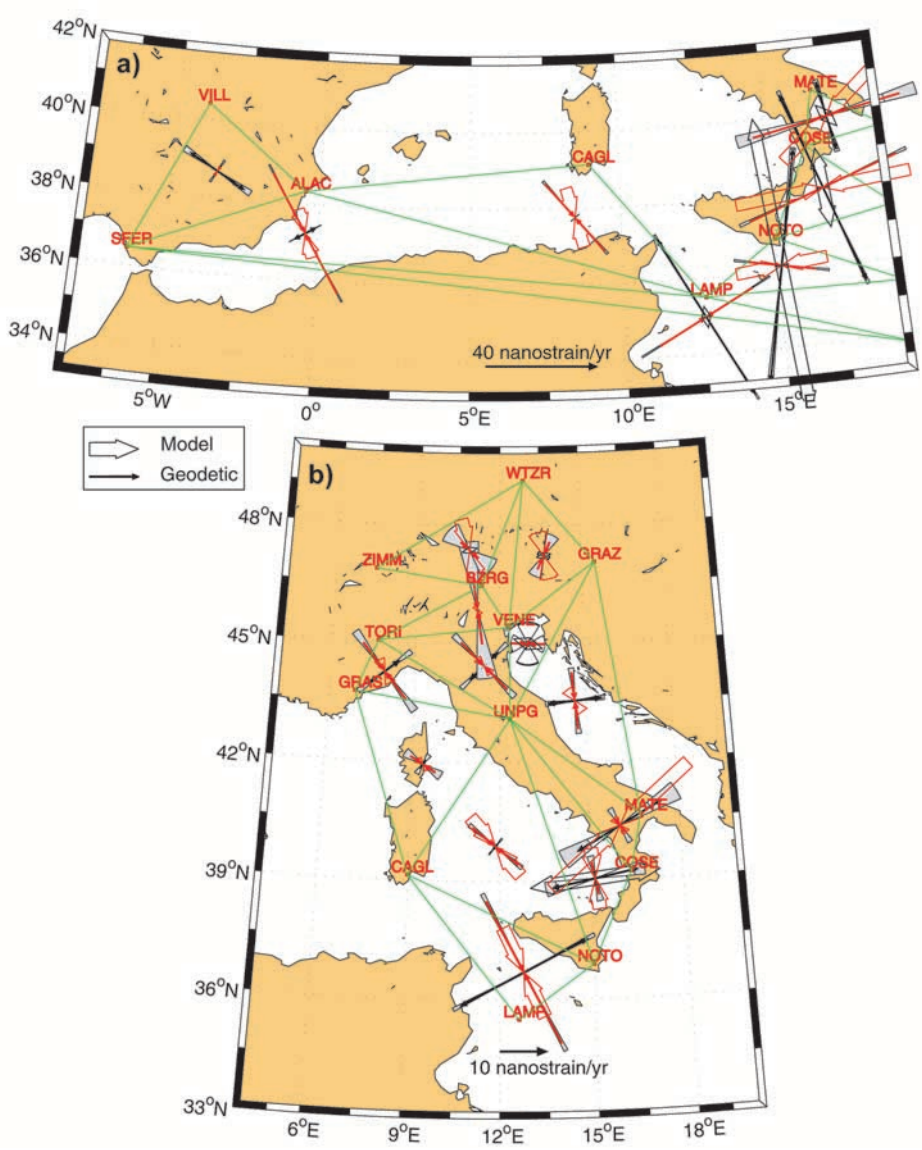

Figure 15. Horizontal principal strain rates: geodetic ones (solid arrows) and modeled ones (open arrows) resulting from model C, with the associated errors. Extension is represented by black and compression is represented by red for (a) western Mediterranean, (b) central Mediterranean, (c) Aegean region, and (d) Anatolian Peninsula.

and geodetic velocity direction of MATE. The geodetic E-W extension UNPG-NOTO-MATE, not reproduced by the model, agrees well with the extensional tectonics perpendicular to the Apenninic chain, indicated by the normal fault events (yellow bars) appearing in the WSM2000 map in Figure 5. The observed extension perpendicular to the chain could indicate that subduction is also active underneath the central Apennines, a process that has not been parameterized in the modeling. This would explain the failure of the model to reproduce the geodetic and WSM2000 extension. In proximity to the Calabrian Arc, the principal strain rate is extensional (UNPG-COSE-NOTO), with complete coherence between geodetic and modeled eigendirections and eigenvalues, and roughly perpendicular to the arc, probably indicating rollback of the arc itself. This pattern is in agreement with the radial extension stress regime proposed by *Rebaï et al.* [1992] which appears also in the WSM2000 map in the Calabrian Arc region, indicated by the yellow bars parallel to the arc. From the geodetic strain rate the pentagon GRAS-TORI-UNPG-NOTO-CAGL portrays a NW compression as the dominant mechanism, changing into dominant ENE extension in the triangles CAGL-NOTO-LAMP and UNPG-COSE-NOTO. The model fits very well all these features, except the high ENE extension in the triangle CAGL-NOTO-LAMP. The dominant NW compression in the pentagon above is also evident in the WSM2000 map, via the thrust events in western Sicily and in the Ligurian coast of Italy (blue bars).

[42] If we move to the north, in northern Italy and in the Alpine front, we notice a deterioration in the quality of the geodetic strain, which is characterized by larger errors. In both the geodetic and modeled strain rate values we notice a substantial reduction with respect to the southern values, in agreement with the reduction of deformation from south to

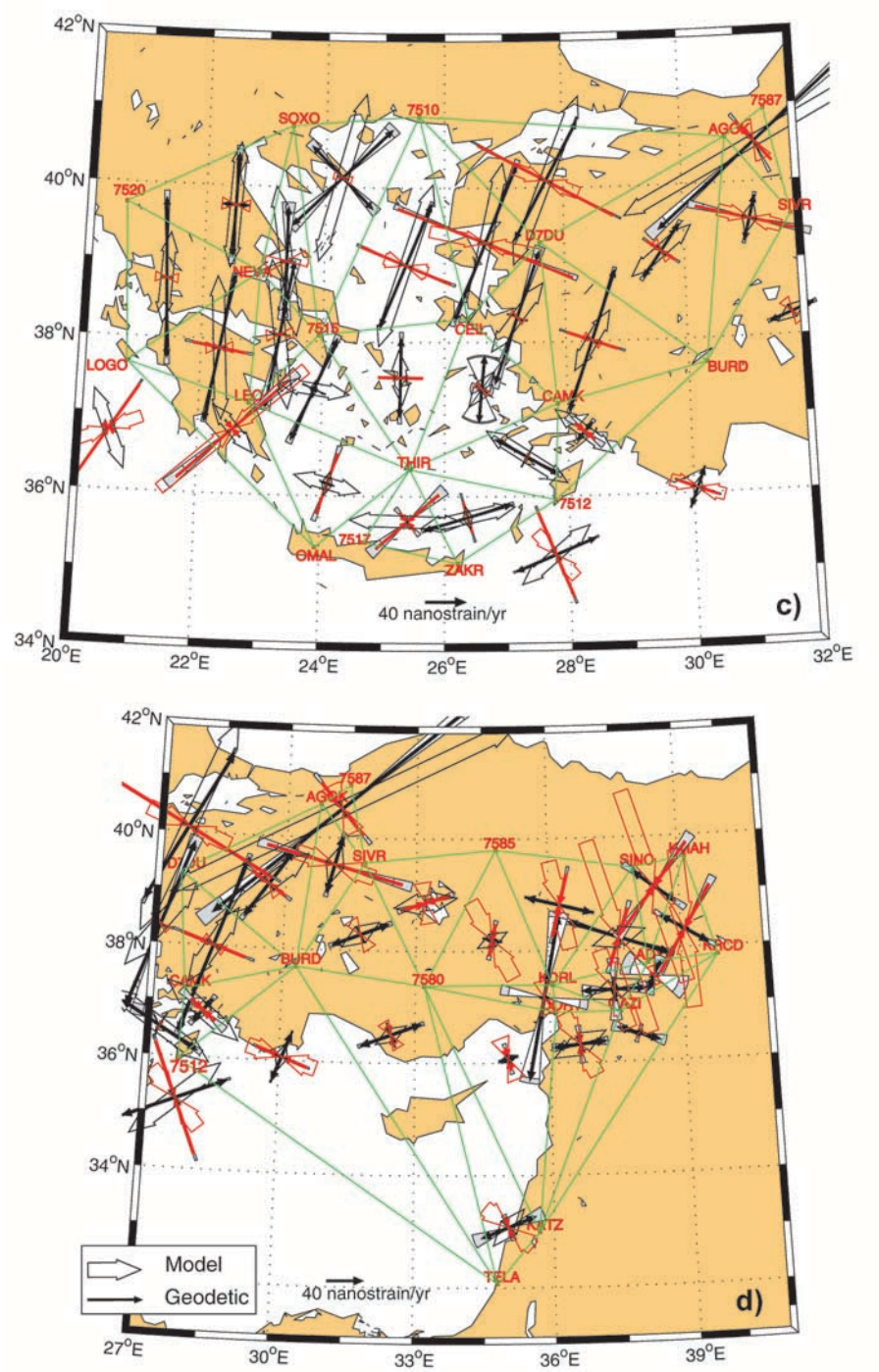

Figure 15. (continued)

north due to the larger distance from the Africa-Eurasia collision and subduction zones. The eigendirections are generally well reproduced; the fit is poor for both TORI-VENE-UNPG and VENE-GRAZ-UNPG, with a 90° mismatch in this second triangle in the eigendirection and the modeling predicting essentially zero strain rates in the first one. This may be due to limitations in the model or to the quality of the geodetic strain, both possibly related to the small size of the strain rates in the area or to the difficulties in dealing with small-scale active tectonic features. There may also be effects associated with the hydrological cycle of the crust. In the triangle TORI-VENE-UNPG the geodetic compression fits very well with the thrusts events (blue bars) in the corresponding region of the WSM2000 map. Within the pentagon ZIMM-WTZR-GRAZ-VENE-BZRG the style of the compressive strain rates is well reproduced by the modeling, both in the eigendirections and eigenvalues. Both the geodetic data and geophysical model agree with the WSM2000 map that portrays a cluster of thrust events in the region corresponding to the triangle WZTR-GRAZ-VENE. A mismatch between the geodetic and modeled strain rates occurs within the two triangles VENE-GRAZ-UNPG and

GRAZ-MATE-UNPG, denoting the Adriatic sector. In this sector, west directed extension is predicted rather than compression, for the first triangle, and in the second triangle, E-W extension is not well reproduced.

[43] In the Aegean region (Figure 15c) we obtain a general improvement in the coherence between the eigendirections and eigenvalues obtained from the geodetic data and from the numerical modeling relative to the results of Figures 15a and 15b. Extension, in the NNE direction, is the dominant mechanism, expected to induce a nearly north trending normal faulting deformation, which is, in fact, the major feature portrayed by the WSM2000 map in the Aegean region (Figure 5). This extension fits well with the idea that the suction force induced by the negatively sinking slab in the Aegean is a major driving mechanism. In considering the details of this widespread extensional pattern we notice that the largest deviation in the eigendirection occurs in the triangles LEON-7515-TWR in Greece and CAMK-BURD-7512 in western Anatolia, with a mismatch of $\sim 90^\circ$ and in SOXO-7510-7515, with a mismatch of $\sim 30^\circ$. Except for these three triangles, the geodetic and modeled strain rates eigendirections are in good agreement, both in Greece and western Anatolia. The eigenvalues are also in fairly good agreement, but we notice that when a mismatch occurs, the numerical model has the tendency to underestimate the geodetic extension, as for example in the triangle 7520-NEZA-LOGO in eastern Greece or in the two triangles in western Anatolia, D7DU-CAMK-CEIL and D7DU-BURD-CAMK. The model has difficulty reproducing the isotropic extension for SOXO-7510-7515. In general, we obtain a fairly good agreement between the eigendirections and largest eigenvalues. Moving to the east, the NNE extension in Greece and Aegean region has the tendency to rotate to NE in Anatolia. In concert with this rotation in the eigendirection of the extension, we notice that compression at right angles with respect to the previous direction, namely, WNW compression, has the tendency to become the dominant mechanism once we move to the east in Anatolia. Drawing a parallelism with the driving mechanism of extension in the Aegean region, the increase in compression to the east in Anatolia fits well with the idea that the push from the Arabian plate is a major controlling mechanism in the easternmost part of Anatolia. It is thus clear that the peculiar pattern of extension and compression is due to the combined effects of suction induced by deep Aegean subduction and by the push of Arabia. This predominant extension in the Aegean Sea and the increasing compression to the east also explain the tectonic regime observed in the WSM2000 map: normal faulting in the Aegean Sea and predominantly strike slip in the east.

[44] In proximity to the Hellenic Arc, the modeled extension parallel to the arc overestimates the geodetic one, and we notice a considerable geodetic compression perpendicular to the arc, especially in its western part, which is underestimated by the model. North of Crete, we notice compression in the geodetic strain perpendicular to the arc and extension parallel to it, in agreement with the numerically modeled eigendirections (LEON-OMAL-TWR; TWR-ZAKR-7512). The model reproduces the compression perpendicular to the arc south of Greece (LOGO-LEON-OMAL), but not north of Crete. The extensional strain rate regime parallel to the arc resulting from the modeling is visible in the WSM2000 map. We mention this case as a situation in which there is a better agreement between the model and the stress data than between the model and the geodetic data or between the geodetic and the stress data. In this arc region the worst fit occurs in the westernmost part of Crete (LEON-OMAL-TWR), where predominantly WNW extension is modeled rather than NNE geodetic compression. East of Crete (TWR-7512-ZAKR) the modeled extension becomes consistent with observations.

[45] Deviations between the eigendirections are observed west of the Peloponnesus and east of Crete, certainly due to edge effects at the subduction zone, where the smoothing of the applied velocities that simulate the suction force are based on the work by *Negredo et al.* [1999]. These results show that the major effects of the Aegean subduction are correctly reproduced, while at the edge of the plate the modeled strain rate is affected by local three-dimensional effects. In spite of this limitation, we notice that the intensity of the geodetic strain rate is well reproduced, denoting compression directed outward from the subduction zone and extension along the hinge line of the subduction. The maximum geodetic and modeled strain rate eigenvalues of $\sim 10^2$ nanostrain yr^{-1}, located in northwestern Anatolia inproximity to the NAF, agree well with the maximum geodetic strain rate obtained by *Ward* [1998] from the Aegean-Anatolian region. The pattern of geodetic and modeled strain release by *Ward* [1998] is not comparable in detail with ours because of the larger set of geodetic data considered and to the higher spatial resolution in our study.

[46] Figure 15d portrays the geodetic and modeled strain rate for Anatolia. The modeled eigendirections are best reproduced in the western part, with a rotation from NNE (CAMK-D7DU-BURD) to NE(AGOK-SIVR-7587), when we move from a longitude of 28° to 32° in good agreement with the largest geodetic eigenvalues denoting extension. Both the geodetic and modeled strain rates are in complete agreement with the cluster of normal fault events in western Anatolia, denoting extension in the NNE direction (WSM2000 map, Figure 5). From west to east, we notice, at least for the largest eigenvalue, a change from dominant extension to dominant compression, both in the model and in the geodetic data. Furthermore, there is an intermediate zone of reduced strain rates, centered approximately at 33°E, in which the dominant NE extension in the west, although reduced, changes into NE compression when we move to the east. The model reproduces well the reduction in the strain rates eigenvalues observed in the data, but in the triangle SIVR-7585-7580, in the center of Anatolia, the model eigenvectors are rotated by 90° with respect to the geodetic one, a negative result which is not unexpected because of the size of the strain rate. In the center of Anatolia the model thus reproduces very well the reduction in the strain rate and the transition from extension in the west to compression in the east, but the model fails to model the eigendirections in the center of this zone. The reduction in the strain rates is well imaged in the WSM2000 map by the lower number of stress data. In the eastern part, NNW compression is the dominant mechanism, in agreement with the idea of a dominant role played by the push of Arabia. The magnitude of the largest eigenvalue is generally overestimated by the model, clearly controlled by the push of the Arabian plate. The model fails to reproduce the extension

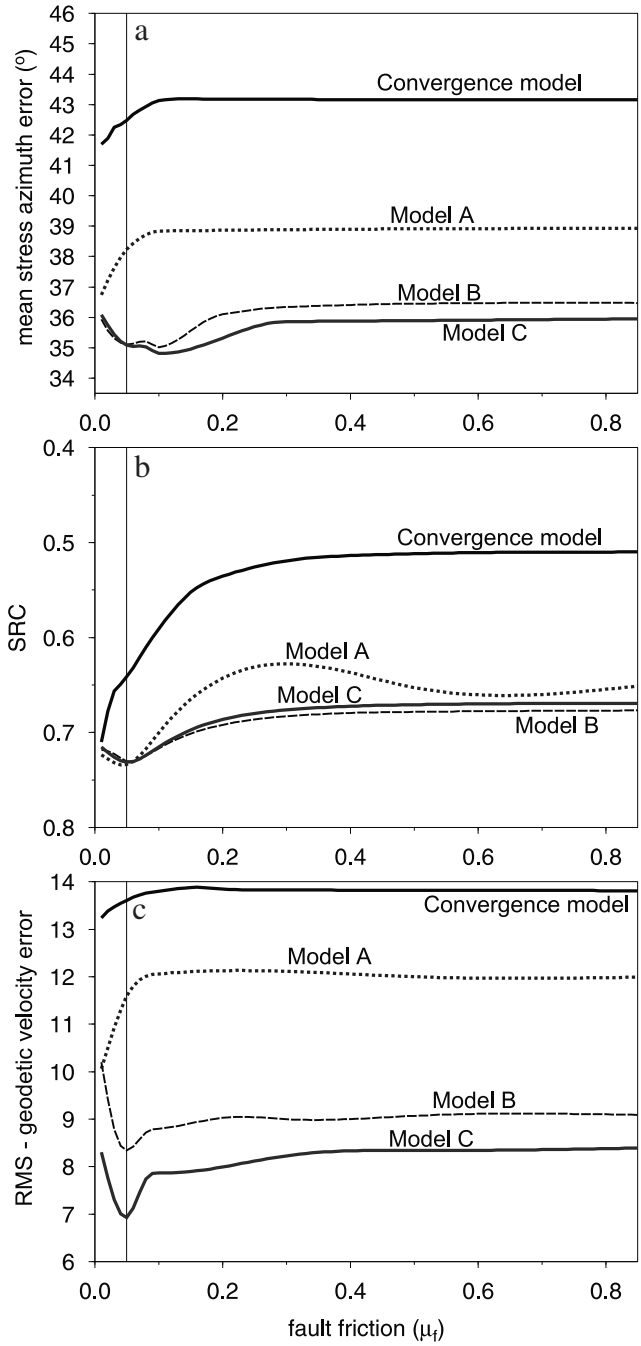

Figure 16. Testable predictions as a function of the fault friction coefficient for different models. (a) Mean stress azimuth error, deviation of the maximum horizontal compression direction between the model and the data (WSM2000). (b) Strain rate correlation coefficient SRC (equation (8)) between the modeled and the seismic strain rates. (c) Misfit between the geodetic and the modeled velocities (equation (9)). Best models are those with low mean stress azimuth and geodetic error but high correlation with the seismic strain rate (SRC).

observed in the data; while reproducing the largest eigenvalues, the model has difficulties in reproducing the smallest ones. In the eastern part of Anatolia the geodetic eigendirection is rotated counterclockwise with respect to the modeled one. This discrepancy in the eigendirections could be due to edge effects, since this region is close to the boundary where the velocity conditions are applied (Figure 6). Comparison with the WSM2000 map is not as robust as in the western part of Anatolia: a single stress datum in the easternmost region denotes thrusting, with an eigendirection roughly in agreement with the geodetic observation and modeled NE compression.

[47] As a general comment on Figure 15, we notice that once converted into the strain rates per second, as in Figures 3, 7, 11, and 13, we obtain a level of $\sim 10^{-15}$ s^{-1} in the modeled and geodetic strain rates, which are thus coherent in magnitude, both being higher than the seismic strain rate. This general finding is not unexpected, since the geodetic strain is the sum of the deformation released by earthquakes and of that due to ductile creep of the crust and lithosphere. This explains why the geodetic strain may be larger than the seismic one. The short time window spanned by the seismic catalogs could be another cause for the seismic strain being generally lower than the geodetic and modeled ones. These findings and conclusions are consistent with those drawn by *Ward* [1998]. The coherence between the modeled and geodetic strain reveals the capability of our model to reproduce the flow properties of the crust and lithosphere and to provide an estimate of the release of seismic deformation. A comparison of the magnitudes of the modeled strain rate (Figure 15) with the seismic strain rate (Figure 3) indicates a good correlation, with high values in southern Italy, decreasing to the north, high strain rate in the Aegean, decreasing in central Anatolia, and increasing again near the EAF.

[48] Finally, in Figure 16 we test the correlation between the modeled results and the stress, seismicity and geodetic data while varying the fault friction coefficient. The best performing models are those with the lowest mean stress azimuth error between the eigendirections of the stress tensor retrieved from the WSM2000 map and from our model, the lowest geodetic velocity RMS error (equation (9)) and the highest SRC values (equation (8)). The worst performing models are those in which the only tectonic mechanism is the Africa/Arabia versus Eurasia convergence which yields the largest errors in the mean azimuth of the stress eigendirections and the lowest SRC. A major improvement in all measures of fit results from the inclusion of subduction from the convergence model (solid) toward the cluster of curves referring to the various subduction models A-C (dotted, dashed, and gray). Detailing the different behavior of the subduction models, we notice that the inclusion of the deep Aegean subduction is responsible for a major reduction in the mean stress azimuth and geodetic velocity error, from model A to model B but leaves the SRC relatively unaffected. The smoothing of the suction and slab pull velocities at the edge of the subduction zones substantially improve the RMS of the geodetic velocity from model B to model C, with a smaller improvement in the mean stress azimuth error. The SRC is unaffected by the smoothing of the subduction velocities at the edges.

[49] When we consider the effects of varying the fault friction coefficient, we notice that this value primarily impacts the SRC, which strongly prefers relatively low values. The RMS geodetic velocity and mean stress azimuth error prefer a reduction in the fault friction coefficient from

0.85 to values closer to 0.05, in agreement with the SRC; however, this preference deteriorates in the range from 0.05 to 0. The best fit for the RMS occurs for 0.05(vertical solid line in Figure 16). This suggests that the plate boundary is 8 times weaker than the continuum lithosphere, a ratio typical for plate boundary faults. *Bird* [1998] studied a global model and proposed a friction coefficient of 0.03 for the plate boundaries; while *Wang and He* [1999] found effective friction of only 0.05 to 0.09 in two subduction zones. Neotectonic studies from California and Alaska [*Bird and Kong*, 1994; *Bird*, 1996] infer a friction coefficient between 0.17 and 0.25; locally, in Cajon Pass the friction appears to be even less [*Lachenbruch and Sass*, 1992]. In a transform plate boundary environment, *Jiménez-Munt et al.* [2001b] found a coefficient of fault friction between 0.1 and 0.15.

6. Conclusions

[50] We found that Africa/Arabia versus Eurasia convergence cannot be the only active tectonic mechanism in the Mediterranean, from Gibraltar to Anatolia. Additional forces, such as slab pull and suction, in the Calabrian and Hellenic Arcs are necessary in order to reproduce, by means of finite element modeling, the geodetic velocity and strain rates patterns, to arrive at a qualitative agreement between the seismic and modeled strain rate patterns, and to reproduce the prominent features of the WSM2000 map, containing the information on the stress field in the studied area. In order to carry into coincidence the geodetic and modeled strain rate tensor quantities in the eastern Mediterranean, Aegean Sea, and Anatolia, the subduction in the Hellenic Arc must be a deep one, as imaged by seismic tomography and not by the relatively shallow hypocentral distribution of earthquakes. On the basis of our results it is not necessary to invoke the mechanism of slab detachment [*Wortel and Spakman*, 2000].

[51] Particular attention has to be drawn to the comparison between the seismic strain rate release and the modeled one because of the shortness of the 100 year time interval spanned by the NEIC catalog and to the steady state deformation pattern of the model, where we assume that the modeled strain rate pattern refers to geological timescales of 10^3–10^6 years. This is probably the cause for the seismic strain rate being generally lower than the modeled and geodetic ones. On the other hand, the geodetic and modeled strain rates are generally in good agreement, which means that the geodetic signal monitors not only the seismic deformation but also the ductile deformation of the crust, which originates from its rheological properties.

[52] From Gibraltar to the east, toward Anatolia, the modeling reproduces the major features visible in the pattern of eigendirections and eigenvalues of the geodetic strain rate tensor, and in the WSM2000 map, namely, NNW compression from Gibraltar to Lampedusa, extension in southern Italy, compression along the Alpine front, the NNE extension in the Aegean and western Anatolia, and finally compression in eastern Anatolia. At the smaller scale, some features are well reproduced, such as the extension parallel to the Hellenic Arc, while some other features, such as the extension perpendicular to the Apenninic chain or the transition zone in central Anatolia between extension and compression, are not, indicating that the effects of local tectonic mechanisms are not properly taken into account.

[53] The modeling also reproduces the main features of the seismic strain rate pattern obtained from the NEIC catalog, namely, the belt of high seismic release in northern Africa and the peculiar shape of the region of high seismic energy release embedding northeastern Italy, Dinarides and southern Italy, the whole Aegean Sea, and western and eastern Anatolia, although the correlation between seismic data and model results must be taken with caution, as discussed above.

[54] The results shown in this study indicate that it is possible to gain a deep insight into the dynamics of the major tectonic mechanisms affecting the Mediterranean once the basic driving processes of plate tectonics are considered within an integrated approach based on model efforts, geodetic and seismic analyses.

[55] **Acknowledgments.** This work is supported by the COFIN2000 project of the Italian Ministry of the Instruction, University and Research, "Active deformation at the northern boundary of Adria." This has also been supported by the contract ASI-1998-2000-Working group on measurements and methods of high precision Space Geodesy. We thank Peter Bird (from UCLA) for SHELLS program and for all his constructive comments. We are indebted for important discussions to Giuliano Panza (from the University of Trieste) and Karim Aoudia (from the International Center of Theoretical Physics (ICTP)). We thank Franco Vespe (from the Italian Space Agency) and Cecilia Sciarretta, Vincenza Luceri, Roberto Devoti, and Marco Fermi (from Telespazio) for their geodetic support. Antonio Villaseñor (from the University of Utrecht) and Ana Negredo (from the University of Madrid) for important discussion and Manel Fernandez (from CSIC, Barcelona),for his support with heat flow data. Finally, we would like to acknowledge Rob Reilinger and Simon McClusky (from MIT) for having provided us with their GPS data in Anatolia. We thank the valuable comments by Jerry Mitrovica, Russell Pysklywec, and an anonymous reviewer.

References

Ambraseys, N. N., and J. A. Jackson, Seismicity and associated strain of central Greece between 1890 and 1988, *Geophys. J. Int.*, *101*, 663–708, 1990.

Anderson, H., and J. Jackson, Active tectonics of the Adriatic regions, *Geophys. J. R. Astron. Soc.*, *91*, 937–983, 1987.

Ansorge, J., D. Blundell, and S. Mueller, Europe's lithosphere-seismic structure, in *The European Geotraverse*, edited by D. Blundell, R. Freeman, and S. Mueller, pp. 33–70, Cambridge Univ. Press, New York, 1992.

Bassi, G., and R. Sabadini, The importance of subduction for the modern stress field in the Tyrrhenian area, *Geophys. Res. Lett.*, *21*, 329–332, 1994.

Bassi, G., R. Sabadini, and S. Rebaï, Modern tectonic regime in the Tyrrhenian area: Observations and models, *Geophys. J. Int.*, *129*, 330–346, 1997.

Bijwaard, H., and W. Spakman, Non-linear global *P*-wave tomography by iterated linearized inversion, *Geophys. J. Int.*, *141*, 71–82, 2000.

Bijwaard, H., W. Spakman, and E. R. Engdahl, Closing the gap between regional and global travel time tomography, *J. Geophys. Res.*, *103*, 30,055–30,078, 1998.

Bird, P., New finite element techniques for modeling deformation histories of continents with stratified temperature-dependent rheology, *J. Geophys. Res.*, *94*, 3967–3990, 1989.

Bird, P., Computer simulations of Alaskan neotectonics, *Tectonics*, *15*, 225–236, 1996.

Bird, P., Testing hypotheses on plate-driving-mechanism with global lithosphere models including topography, thermal structure, and faults, *J. Geophys. Res.*, *103*, 10,115–10,129, 1998.

Bird, P., and X. Kong, Computer simulations of California tectonics confirm very low strength of major faults, *Geol. Soc. Am. Bull.*, *106*, 159–174, 1994.

Catalano, R., C. Doglioni, and S. Merlini, On the Mesozoic Ionian ocean, *Geophys. J. Int.*, *144*, 49–63, 2001.

Cianetti, S., P. Gasperini, M. Boccaletti, and C. Giunchi, Reproducing the velocity and stress fields in the Aegean region, *Geophys. Res. Lett.*, *24*, 2087–2090, 1997.

Clarke, P. J., et al., Crustal strain in central Greece from repeated GPS measurements in the interval 1989–1997, *Geophys. J. Int.*, *135*, 195–214, 1998.

DeMets, C., R. G. Gordon, D. F. Argus, and S. Stein, Effect of recent revisions to the geomagnetic reversal time scale on estimates of current plate motions, *Geophys. Res. Lett.*, *21*, 2191–2194, 1994.

Devoti, R., et al., Geophysical interpretation of geodetic deformations in the central Mediterranean area, in *Plate Boundary Zones*, *Geodyn. Ser.*, vol. 30, edited by S. Stein and J. T. Freymueller, pp. 57–65, AGU, Washington, D. C., 2002.

Dewey, J. F., and A. M. C. Sengor, Aegean and surrounding regions: Complex multiplate and continuum tectonics in a convergent zone, *Geol. Soc. Am Bull.*, *90*, 84–92, 1979.

Doglioni, C., E. Gueguen, F. Sabat, and M. Fernandez, The western Mediterranean extensional basins and the Alpine orogen, *Terra Nova*, *9*, 109–112, 1997.

Du, Z. J., A. Michelini, and G. F. Panza, EurID: A regionalized 3-D seismological model of Europe, *Phys. Earth Planet. Inter.*, *105*, 31–62, 1998.

Ekström, G., and A. M. Dziewonski, Evidence of bias in estimations of earthquakes size, *Nature*, *332*, 319–323, 1988.

England, P., and P. Molnar, The field of crustal velocity in Asia calculated from Quaternary rates of slip on faults, *Geophys. J. Int.*, *130*, 551–582, 1997.

Fernandez, M., I. Marzan, A. Correia, and E. Ramalho, Heat flow, heat production, and lithospheric thermal regime in the Iberian Peninsula, *Tectonophysics*, *291*, 29–53, 1998.

Frepoli, A., and A. Amato, Spatial variation in stresses in peninsular Italy and Sicily from background seismicity, *Tectonophysics*, *317*, 109–124, 2000.

Giunchi, C., R. Sabadini, E. Boschi, and P. Gasperini, Dynamic models of subduction: Geophysical and geological evidence in the Tyrrhenian Sea, *Geophys. J. Int.*, *126*, 555–578, 1996a.

Giunchi, C., A. Kiratzi, R. Sabadini, and E. Louvari, A numerical model of the Hellenic subduction zone: Active stress field and sea-level changes, *Geophys. Res. Lett.*, *23*, 2485–2488, 1996b.

Gueguen, E., C. Doglioni, and M. Fernandez, On the post-25 Ma geodynamic evolution of the western Mediterranean, *Tectonophysics*, *298*, 259–269, 1998.

Holt, W. E., J. F. Ni, T. C. Wallace, and A. J. Haines, The active tectonics of the eastern Himalayan Syntaxis and surrounding regions, *J. Geophys. Res.*, *96*, 14,595–14,632, 1991.

Irifune, T., and A. E. Ringwood, Phases transformations in a harzburgite composition to 26 GPa: Implications for dynamical behavior of the subducting slab, *Earth Planet. Sci. Lett.*, *86*, 365–376, 1987.

Jackson, J., Partitioning of strike-slip and convergent motion between Eurasia and Arabia in eastern Turkey, *J. Geophys. Res.*, *97*, 12,471–12,479, 1992.

Jackson, J., and D. McKenzie, Active tectonics of the Alpine-Himalayan Belt between western Turkey and Pakistan, *Geophys. J. R. Astron. Soc.*, *77*, 185–246, 1984.

Jackson, J., and D. McKenzie, The relationship between plate motions and seismic tremors, and the rates of active deformation in the Mediterranean and Middle East, *Geophys. J. R. Astron. Soc.*, *93*, 45–73, 1988.

Jiménez-Munt, I., and R. Sabadini, The block-like behavior of Anatolia envisaged in the modeled and geodetic strain rates, *Geophys. Res. Lett.*, *29*, 1978, doi:10.1029/2002GL015995, 2002.

Jiménez-Munt, I., M. Fernandez, M. Torne, and P. Bird, The transition from linear to diffuse plate boundary in the Azores-Gibraltar region: Results from a thin sheet model, *Earth Planet. Sci. Lett.*, *192*, 175–189, 2001a.

Jiménez-Munt, I., P. Bird, and M. Fernandez, Thin-shell modeling of neotectonics in the Azores-Gibraltar region, *Geophys. Res. Lett.*, *28*, 1083–1086, 2001b.

Jonge, M. R., M. J. R. Wortel, and W. Spakman, Regional scale tectonic evolution and the seismic velocity structure of the lithosphere and upper mantle: The Mediterranean region, *J. Geophys. Res.*, *99*, 12,091–12,108, 1994.

Kahle, H.-G., M. Cocard, Y. Peter, A. Geiger, R. Reilinger, A. Barka, and G. Veis, GPS-derived strain rate field within the boundary zones of the Eurasian, African and Arabian Plates, *J. Geophys. Res.*, *105*, 23,353–23,370, 2000.

Kiratzi, A., and C. Papazachos, Active deformation of the shallow part of the subducting lithospheric slab in the southern Aegean, *J. Geodyn.*, *19*, 65–78, 1995.

Kirby, S. H., Rheology of the lithosphere, *Rev. Geophys.*, *21*, 1458–1487, 1983.

Kong, X., and P. Bird, Shells: A thin-plate program for modeling neotectonics of regional or global lithosphere with faults, *J. Geophys. Res.*, *100*, 22,129–22,131, 1995.

Kostrov, V., Seismic moment and energy of earthquakes, and seismic flow of rock, *Izv. Acad. Sci. USSR Phys. Solid Earth*, *1*, 23–44, 1974.

Lachenbruch, A. H., and J. H. Sass, Heat flow from Cajon Pass, fault strength, and tectonic implications, *J. Geophys. Res.*, *97*, 4995–5015, 1992.

Le Pichon, X., and J. Angelier, The Hellenic Arc and trench system: A key to the neotectonic evolution of the eastern Mediterranean area, *Tectonophysics*, *60*, 1–42, 1979.

Lundgren, P., D. Giardini, and R. M. Russo, A geodynamic framework for eastern Mediterranean kinematics, *Geophys. Res. Lett.*, *25*, 4007–4010, 1998.

Marotta, A. M., M. Fernandez, and R. Sabadini, The onset of extension during lithospheric shortening: A two-dimensional thermomechanical model for lithospheric unrooting, *Geophys. J. Int.*, *139*, 98–114, 1999.

McClusky, S., et al., Global Positioning Systemconstraints on plate kinematics and dynamics in the eastern Mediterranean and Caucasus, *J. Geophys. Res.*, *105*, 5695–5719, 2000.

McKenzie, D. P., Plate tectonics of the Mediterranean region, *Nature*, *226*, 239–243, 1970.

Meijer, P. T., and M. J. R. Wortel, The dynamics of motion of the South American plate, *J. Geophys. Res.*, *97*, 11,915–11,931, 1992.

Meijer, P. T., and M. J. R. Wortel, Temporal variation in the stress field of the Aegean region, *Geophys. Res. Lett.*, *23*, 439–442, 1996.

Mueller, B., J. Reinecker, O. Heidbach, and K. Fuchs, The 2000 release of the World Stress Map, 2000. (Available at www.world-stress-map.org)

Negredo, A. M., R. Sabadini, and C. Giunchi, Interplay between subduction and continental convergence: A three-dimensional dynamic model for the Central Mediterranean, *Geophys. J. Int.*, *131*, F9–F13, 1997.

Negredo, A. M., R. Sabadini, G. Bianco, and M. Fernandez, Three-dimensional modeling of crustal motions caused by subduction and continental convergence in the central Mediterranean, *Geophys. J. Int.*, *136*, 261–274, 1999.

Papazachos, B. C., V. G. Karakostas, C. B. Papazachos, and E. M. Scordilis, The geometry of the Wadati-Benioff zone and lithospheric kinematics in the Hellenic Arc, *Tectonophysics*, *319*, 275–300, 2000.

Piromallo, C., and A. Morelli, Imaging the Mediterranean upper mantle by *P*-wave travel time tomography, *Ann. Geofis.*, *4*, 963–979, 1997.

Platt, J. P., and R. L. M. Vissers, Extensional collapse of thickened continental lithosphere: A working hypothesis for the Alboran Sea and Gibraltar Arc, *Geology*, *17*, 540–543, 1989.

Pollack, H. N., S. J. Hurter, and J. R. Johnson, Heat loss from the Earth's interior: Analysis of the global data set, *Rev. Geophys.*, *31*, 267–280, 1993.

Rebaï, S., H. Philip, and A. Taboada, Modern tectonics stress field in the Mediterranean region: Evidence for variation in stress directions at different scales, *Geophys. J. Int.*, *110*, 106–140, 1992.

Royden, L. H., Evolution of retreating subduction boundaries formed during continental collision, *Tectonics*, *12*, 629–638, 1993.

Seber, D., M. Barazangi, B. Tadili, M. Ramdani, A. Ibenbrahim, and D. Bensari, Three-dimensional upper mantle structure beneath the intraplate atlas and interplate Rif mountains of Morocco, *J. Geophys. Res.*, *101*, 3125–3138, 1996.

Spakman, W., S. van der Lee, and R. D. van der Hilst, Travel-time tomography of the European-Mediterranean mantle down to 1400 km, *Phys. Earth Planet. Inter.*, *79*, 3–74, 1993.

Taymaz, T., J. Jackson, and D. McKenzie, Active tectonics of the north and central Aegean Sea, *Geophys. J. Int.*, *106*, 433–490, 1991.

Wang, K., and J. He, Mechanics of low-stress forearcs: Nankai and Cascadia, *J. Geophys. Res.*, *104*, 15,191–15,205, 1999.

Ward, S. N., Constraints in the seismotectonics of the central mediterranean from very long baseline interferometry, *Geophys. J. Int.*, *117*, 441–452, 1994.

Ward, S. N., On the consistency of earthquake moment release and space geodetic strain rates: Europe, *Geophys. J. Int.*, *135*, 1011–1018, 1998.

Wortel, M. J. R., and W. Spakman, Subduction and slab detachment in the Mediterranean-Carpathian region, *Science*, *290*, 1910–1917, 2000.

Zeck, H. P., Betic-Rif orogeny: Subduction of Mesozoic Tethys lithosphere under eastward drifting Iberia, slab detachment shortly before 22 Ma, and subsequent uplifting and extensional tectonics, *Tectonophysics*, *254*, 1–16, 1996.

Zerbini, S., B. Richter, M. Negusini, C. Romagnoli, D. Simon, F. Domenichini, and W. Schwahn, Height and gravity variations by continuous GPS, gravity and environmental parameter observations in the southern Po Plain, near Bologna, Italy, *Earth Planet. Sci. Lett.*, *192*, 267–279, 2001.

G. Bianco, Agenzia Spaziale Italiana, Centro di Geodesia Spaziale "G. Colombo," Matera, Italy.

A. Gardi, IRSN, Fontenay-aux-Roses, France.

I. Jiménez-Munt and R. Sabadini, Sezione Geofisica, Dipartimento di Scienze della Terra, Università di Milano, Via Cicognara 7, I-20129 Milan, Italy. (ivone.jimenez@unimi.it)